IEEE Access
Multidisciplinary | Rapid Review | Open Access Journal

Received October 3, 2020, accepted October 13, 2020, date of publication October 20, 2020, date of current version November 13, 2020.

Digital Object Identifier 10.1109/ACCESS.2020.3032419

Discontinuous PWM Techniques of Three-Leg Two-Phase Voltage Source Inverter for Sonar System

JAEHYUK CHOI[1], (Student Member, IEEE), DONG-HUN LEE[2], AND HYUNGSOO MOK[1], (Member, IEEE)

[1]Electric Machine and Power Electronics Laboratory, Konkuk University, Seoul, South Korea
[2]Agency for Defense Development, Chinhae, South Korea

Corresponding author: Hyungsoo Mok (hsmok@konkuk.ac.kr)

This work was supported by the Agency for Defense Development (Research Service for Receiving Miniaturization Technology for Small Aquatic Motion) under Grant 20160927524-00.

ABSTRACT Pulse width modulation (PWM) methods are important for the detection performance of a sound navigation and ranging (sonar) system because they determine the output noise of the system. However, only few studies have been conducted on PWM methods for reducing harmonics of a sonar system. In this study, we propose a discontinuous pulse width modulation (DPWM) method for three-leg two-phase (3L2P) inverters. Further, we derive a complete harmonic solution for a double-variable-controlled waveform for the proposed DPWM and conventional continuous pulse width modulation (CPWM) methods. Using these harmonic solutions, we analyze the normalized weighted total harmonic distortion (NWTHD) characteristics according to the modulation index (MI) of the inverter and phase difference of the output voltage for each method. Further, based on the results, we present a superiority map between the conventional CPWM and proposed DPWM methods in terms of the NWTHD. An NWTHD measurement experiment was performed to verify the proposed method. The experiment included additional evaluations of switch losses, phase difference variability, and voltage utilization, which are important factors for sonar systems. This is because improving only NWTHD performance while other factors degrade is not very useful. The results of the experiment confirm that the NWTHD for the proposed DPWM method was 92.5% of that for the conventional CPWM method. We confirm that the mean error of the NWTHD between the analytical and experimental values under similar conditions was less than ∼2.2%. In addition, it was verified that the important factors, except NWTHD, were the same throughout additional experiments. Therefore, if the CPWM or DPWM method is selected based on the proposed selection criteria, realizing advantageous operation in terms of the NWTHD is possible.

INDEX TERMS Discontinuous pulse width modulation, sonar, voltage source inverter.

I. INTRODUCTION

A sound navigation and ranging (sonar) system converts electrical signals into acoustic signals for emission in a detection area; the acoustic signal reflected from objects is then processed to extract the target information [1]. A focused detection direction of the sonar is determined based on the phase difference between the acoustic signals emitted from each transducer; this technique is called beamforming [2]. The acoustic phase difference is obtained from the electrical phase difference between the output of a power supply such as a voltage source inverter (VSI). Therefore, the detection area of sonar can be adjusted by controlling the electrical phase of the VSI output. However, when a single VSI simultaneously supplies electrical power to multiple sonar transducers in an array structure, the output voltage phase is fixed, and it thereby prevents independent phase control of each transducer. Therefore, independent control using multiple VSIs is necessary to set the phase of the output acoustic signal of every transducer. The configuration of a sonar system is shown in Fig. 1. The system comprises a full-bridge VSI (using two switch legs) to control the output phase of each

The associate editor coordinating the review of this manuscript and approving it for publication was Atif Iqbal.

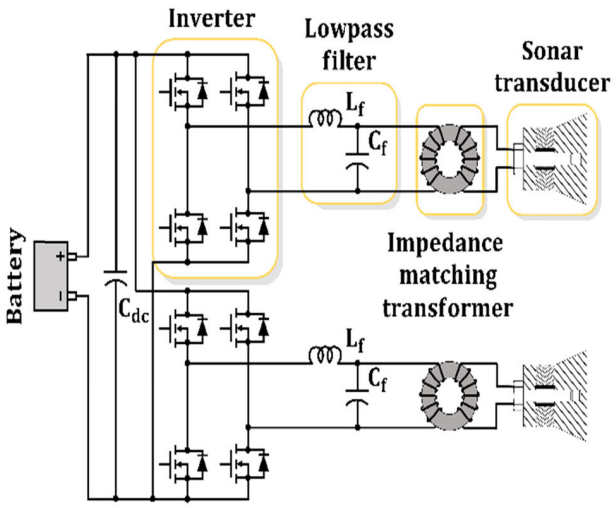

FIGURE 1. Sonar system using four-leg two-phase VSI.

sonar transducer or groups of transducers. When the number of transducers (or groups of transducers) increases by n, the number of legs increases by $2n$, which hinders scalability because the installation space is limited owing to the tendency of the industry toward miniaturization (e.g., in case of medical equipment, weapons, fishing, and so on) [3]. Thus, if less than $2n$ legs can be used for control, the total number of legs and volume occupied by the VSI in the sonar system can be reduced. This reduction in the VSI volume enables an increase in battery space for power supply, which increases the operating time per charge.

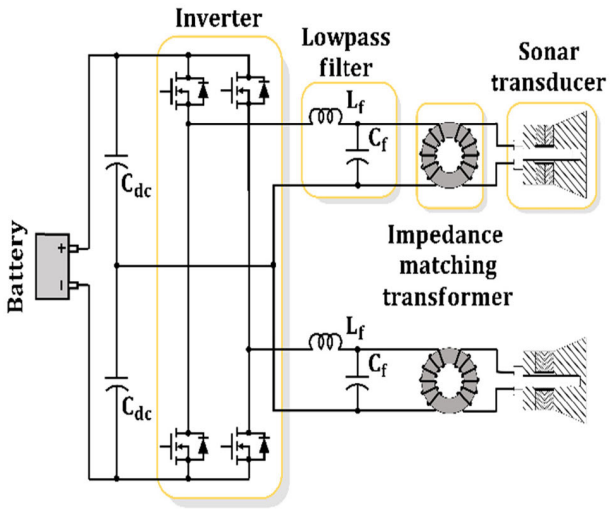

FIGURE 2. Sonar system using two-leg two-phase VSI.

A two-leg two-phase (2L2P) configuration has been used for reducing the number of used legs per phase [4]–[6]. The 2L2P configuration is shown in Fig. 2, where two split capacitors that divide the DC link voltage are connected in series. There is an error because the capacitances of the split capacitors are not equal. Therefore, balancing resistors are used to divide the DC link voltage equally, which results in unnecessary power loss [7]. This power dissipation leads to wastage of the limited energy of batteries; if the capacitance of the split capacitor is not sufficiently large (because of size limitations), the magnitude of the output voltage fluctuates by the charge and discharge of the capacitor during driving of the system [8]. This fluctuation in the output voltage reduces the quality of the acoustic signal, which reduces the target imaging resolution of the sonar system. Further, as the DC link voltage is halved and applied to the load, the voltage utilization decreases [7]. Therefore, the 2L2P configuration is not suitable for a sonar transducer.

To solve this problem, a three-leg two-phase (3L2P) configuration is introduced [9], which uses a single capacitor instead of a split capacitor; the one additional leg. called a common leg, is connected to neutral point (connected point of two split capacitors in the 2L2P configuration) and controls the neutral-point voltage. In this configuration, no output voltage fluctuation occurs as no split capacitor is used, which eliminates the corresponding voltage error. Table 1 lists a comparison between each VSI topology for the sonar system. Moreover, when using the 3L2P configuration, the common leg connects one end of each load to the same leg. This leg can be controlled to increase voltage utilization. Therefore, a PWM method for appropriately controlling 3L2P VSI is required. Additionally, as the acoustic signal is generated by the voltage input to the sonar transducer, the more the input voltage contains harmonics, the lower will be the quality of the acoustic signal. An accident risk exists when detection failure occurs due to such performance degradation. Therefore, it is important to study the PWM method for a sonar system.

Recently, different modulation strategies have been proposed for the 3L2P VSI. Several studies have examined sinusoidal pulse width modulation (PWM) [10], [11]. In [9], space vector PWM was used to generate a symmetrical phase voltage for increasing DC link voltage utilization. For unbalanced systems, such as two-phase induction motors, asymmetrical phase voltage generation that changes the locations of space vectors according to the asymmetrical phase voltage reference has been devised [12], [13].

However, these studies are applicable to the fixed specific phase difference, and therefore, it cannot be applied to a sonar system operated at phase differences that vary according to the operation strategy. In addition, the maximum voltage utilization is an important factor as it directly affects the maximum output sound pressure. However, previous studies did not consider the maximum voltage utilization according to the variable phase difference; they only considered the fixed phase difference.

Kim and Sul investigated the offset-voltage-type space PWM for four-leg three-phase VSIs to control the neutral voltage of the grid [14]; although this method was developed for the fixed phase difference, it can be directly applied to the 3L2P configuration of the sonar system. However,

TABLE 1. Comparing inverter topologies for sonar systems.

	4L2P	2L2P	3L2P
Phase difference control	Possible	Possible	Possible
Voltage utilization	$2V_{dc}$	V_{dc}	Phase difference dependent
Number of DC link capacitor	1	2	1
balancing resistance	Unnecessary	Necessary	Unnecessary
Number of switches	8	4	6
Cost	High	Low	Medium
Volume	Large	Small	Medium

the method uses continuous PWM (CPWM), in which all semiconductor switches operate continuously at a constant frequency. In the case of the CPWM method, depending on the modulation index (MI), it may be more disadvantageous in terms of total harmonic distortion (THD) than the discontinuous PWM (DPWM) [15]. Therefore, it is necessary to select a method that is advantageous in terms of THD among CPWM and DPWM methods based on the transmission strategy. In addition, because the THD is a multivariate function of the MI and phase difference, mathematical analysis considering both the MI and phase difference is required to derive an optimal operating point based on the PWM method. However, in contemporary research, this mathematical analysis has not been conducted. Therefore, in this study, we derive a complete harmonic solution for a double-variable-controlled waveform for the proposed DPWM and conventional CPWM methods. Based on harmonic solution, we analyze the normalized weighted total harmonic distortion (NWTHD) characteristics according to the MI of the inverter and phase difference of the output voltage for each method.

The rest of this manuscript is organized as follows. In Section II, the maximum voltage utilization based on phase difference is defined by analyzing the basic operation of the 3L2P VSI and the existing offset-voltage type CPWM method. Thereafter, an offset-voltage type DPWM method considering variable phase difference is proposed, and various applicable phase differences, according to operating conditions, are defined. A complete harmonic solution for each PWM method and an optimal operating point in terms of the THD is derived and presented in Section III. Finally, the THD for each PWM method is experimentally evaluated under the same level of switch losses and output conditions. The optimal operating points derived from Section III are compared, and the verification is provided in Section IV.

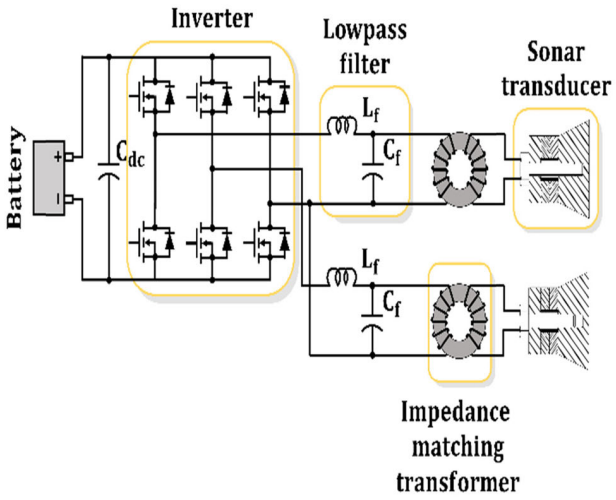

FIGURE 3. Sonar system using three-leg two-phase VSI.

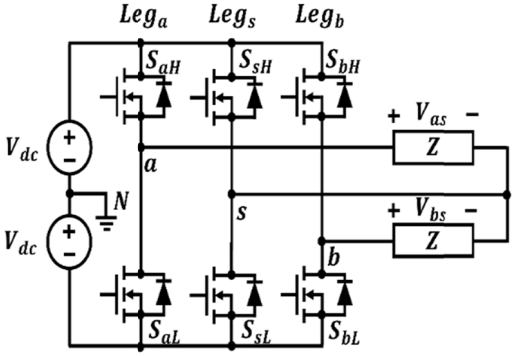

FIGURE 4. Three-leg two-phase VSI.

II. PWM STRATEGIES OF THREE-LEG TWO-PHASE VOLTAGE SOURCE INVERTER FOR SONAR

Fig. 4 shows the configuration of the circuit depicted in Fig. 3 for analyzing the VSI output voltage. In Fig. 4, N represents the ground; V_{dc} is the DC link voltage; and a, b, and s are the output nodes of Leg_a, Leg_b, and Leg_s, respectively. In addition, pole voltages V_{aN}, V_{bN}, and V_{sN}, which are the output voltages from the VSI legs, represent the potential difference between the output node and ground N according to the respective switch states. Moreover, phase voltages V_{as} and V_{bs} applied to load Z are determined by the potential difference between the pole voltages given by

$$\begin{aligned} V_{as} &= V_{aN} - V_{sN} \\ V_{bs} &= V_{bN} - V_{sN} \end{aligned} \tag{1}$$

and the phase voltages have independent constraints as expressed by

$$-2V_{dc} \le V_{as}, V_{bs} \le 2V_{dc} \tag{2}$$

From (1), the pole voltages are given by

$$\begin{aligned} V_{aN} &= V_{as} + V_{sN} \\ V_{bN} &= V_{bs} + V_{sN} \end{aligned} \tag{3}$$

If the required phase voltage is selected, the pole voltages are determined by V_{sN}. Therefore, as the 3L2P VSIs have an extra degree of freedom—provided by Leg_s—the voltage utilization increases by controlling V_{sN}. For example, if V_{sN} is set to 0 and the magnitude of V_{as} and V_{bs} (i.e., phase difference equal to 0), the maximum output voltages of V_{as} and V_{bs} are limited to $V_{\rm dc}$. However, when V_{sN} is set to $-V_{\rm dc}$, the maximum V_{as} and V_{bs} are $2V_{\rm dc}$, which is a two-fold increase.

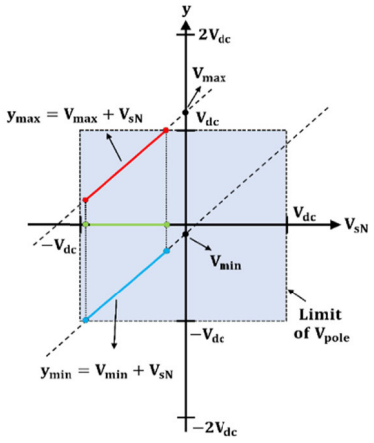

FIGURE 5. Range of pole voltage V_{sN} (CPWM).

In Fig. 5, $V_{\rm max}$ and $V_{\rm min}$ are given by max (V_{as}, V_{bs}) and min (V_{as}, V_{bs}), respectively. $y_{\rm max}$ and $y_{\rm min}$ are the sum of $V_{\rm max}$ and $V_{\rm min}$ with V_{sN}, respectively. Therefore, the trajectory of $y_{\rm max}$ and $y_{\rm min}$ in Fig. 5 represents the pole voltage trajectory to satisfy the phase voltage when V_{sN} changes in the state where the values of $V_{\rm max}$ and $V_{\rm min}$ are determined. Since the maximum value of the pole voltage must satisfy

$$-V_{\rm dc} \le V_{aN}, \quad V_{bN}, \; V_{sN} \le V_{\rm dc}, \tag{4}$$

the pole voltage should exist only within the square box in Fig. 5. Therefore, the available range of V_{sN} is determined according to $V_{\rm max}$ and $V_{\rm min}$. For example, assuming that V_{aN} is $1.5V_{\rm dc}$ and V_{bN} is $-0.2V_{\rm dc}$, respectively, if V_{sN} exceeds $-0.5V_{\rm dc}$, the value of V_{aN} becomes greater than $V_{\rm dc}$; if V_{sN} is less than $-0.8V_{\rm dc}$, V_{bN} becomes less than $-V_{\rm dc}$. Consequently, V_{sN} can be varied in the limited range from $-0.8V_{\rm dc}$ to $-0.5V_{\rm dc}$.

A. CONVENTIONAL CPWM USING OFFSET VOLTAGE FOR THREE-LEG TWO-PHASE VSI

The available range of V_{sN} is limited by V_{as} and V_{bs}, and this can be summarized according to the relationship with $V_{\rm max}$ and $V_{\rm min}$ as

$$-V_{\rm dc} - V_{\rm min} \le V_{sN} \le V_{\rm dc} - V_{\rm max} \tag{5}$$

In addition, V_{sN} must also satisfy the common limit of pole voltage as given in (4), which ensures that 1) both $V_{\rm max}$ and $V_{\rm min}$ are positive; 2) both $V_{\rm max}$ and $V_{\rm min}$ are negative; and 3) $V_{\rm max}$ and $V_{\rm min}$ have different polarities. If they are different, the value of V_{sN} can be determined basis the above three cases.

For case 1, the maximum value of V_{sN} limited by $V_{\rm max}$ is within the limit of (4); however, the minimum value of V_{sN} limited by $V_{\rm min}$ exceeds the limit of (4) in all possible ranges of $V_{\rm min}$. Therefore, in this case, V_{sN} is in the range of $-V_{\rm dc}$ to $V_{\rm dc}V_{\rm max}$, and $V_{\rm min}$ is not valid for determining V_{sN}. Conversely, in case 2, the range of V_{sN} is limited from $-V_{\rm dc}V_{\rm min}$ to $V_{\rm dc}$, which is similar to case 1, and therefore, $V_{\rm max}$ is not valid for determining V_{sN}. For case 3, the signs of $V_{\rm max}$ and $V_{\rm min}$ are different, and V_{sN} satisfies the limit of (4) in all combinations of $V_{\rm max}$ and $V_{\rm min}$, which satisfies (2); therefore, the available range is the same as that in (5). When phase voltage is equal to

$$\begin{aligned} V_{as} &= V_m M \cos(\omega_0 t) \\ V_{bs} &= V_m M \cos(\omega_0 t + \delta) \end{aligned} \tag{6}$$

V_{sN} is determined as

$$V_{sN} = \begin{cases} -\dfrac{V_{\rm max}}{2}, & V_{\rm min} > 0 \\ -\dfrac{V_{\rm min}}{2}, & V_{\rm max} < 0 \\ -\dfrac{V_{\rm max} + V_{\rm min}}{2}, & \text{otherwise} \end{cases} \tag{7}$$

according to the sign of the phase voltage [14]. In (6), ω_0 is the angular frequency of the fundamental wave, δ is the electrical phase difference between V_{as} and V_{bs}, M is the MI and $V_{\rm m}$ is the magnitude of the phase voltage. When V_{sN} is determined by (7), it is always set to the median value of the available range of V_{sN}. For example, when V_{as} is $1.5V_{\rm dc}$ and V_{bs} is $-0.7V_{\rm dc}$, according to (5), the available range of V_{sN} is $-0.3V_{\rm dc}$ to $-0.5V_{\rm dc}$, and if V_{sN} is determined according to (7), V_{sN} is set to $-0.4\ V_{\rm dc}$, which is the median value of the range.

Thus, the pole voltage value for synthesizing the phase voltage is distributed without bias in the $V_{\rm dc}$ or $-V_{\rm dc}$ direction.

After determining V_{sN}, the other pole voltages are determined using

$$\begin{aligned} V_{aN} &= V_{as} + V_{sN} \\ V_{bN} &= V_{bs} + V_{sN} \end{aligned} \tag{8}$$

The ON times of upper switches T_a, T_b, and T_s of Leg_a, Leg_b, and Leg_s, respectively, are determined at a PWM carrier frequency of $1/(2T)$ by

$$\begin{aligned} T_a &= \frac{T}{2} + \frac{V_{aN}}{V_{dc}} T \\ T_b &= \frac{T}{2} + \frac{V_{bN}}{V_{dc}} T \\ T_s &= \frac{T}{2} + \frac{V_{sN}}{V_{dc}} T \end{aligned} \tag{9}$$

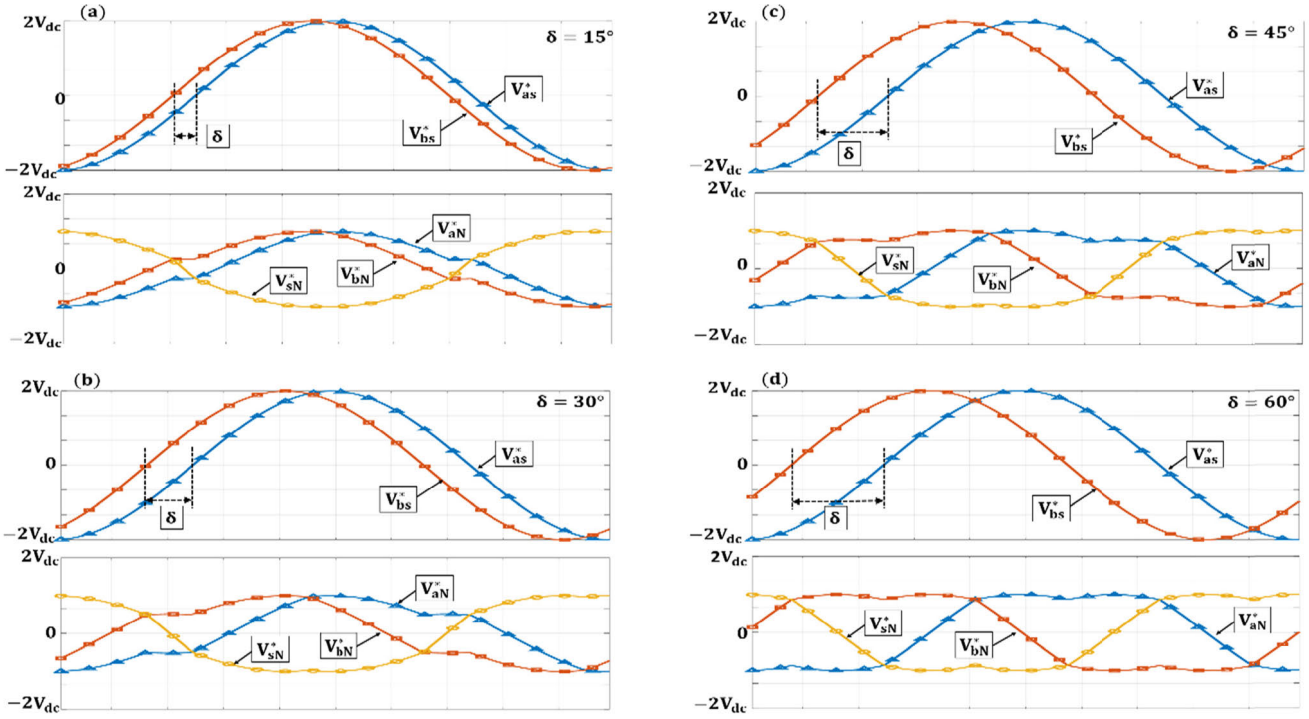

FIGURE 6. Phase voltage and pole voltage reference of CPWM according to phase difference δ ($V_{\mathbf{m}} = 2V_{\mathbf{dc}}$, $M = 1$): (a) $\delta = 15°$, (b) $\delta = 30°$, (c) $\delta = 45°$, (d) $\delta = 60°$.

B. MAXIMUM ACHIEVABLE VOLTAGE IN THREE-LEG TWO-PHASE VSI

If the difference between V_{as} and V_{bs} is equal to or below $2V_{\mathrm{dc}}$, V_{sN} can be controlled within the available range limited by (4), whereas for a difference above $2V_{\mathrm{dc}}$, V_{sN} cannot be controlled and operation occurs in the overmodulation region. To prevent the latter case,

$$V_{as} - V_{bs} \leq 2V_{\mathrm{dc}} \tag{10}$$

must be satisfied. Therefore, when V_{as} and V_{bs} are equal to (6), the magnitude of the difference between V_{as} and V_{bs} is given by

$$2V_m M \sin(\delta) \leq 2V_{\mathrm{dc}} \tag{11}$$

Assuming that the MI is 1, (11) is replaced by

$$V_m \leq \frac{V_{\mathrm{dc}}}{\sin(\delta)} \tag{12}$$

for V_m. Therefore, V_m is defined by V_{dc} and δ. In addition, the phase voltage must also satisfy (2), and thus, the maximum V_m that satisfies both (2) and (12) is equal to

$$V_{\mathrm{m}} = \begin{cases} 2V_{\mathrm{dc}}, & 0° \leq \delta \leq 60° \\ \dfrac{V_{\mathrm{dc}}}{\sin\left(\frac{\delta}{2}\right)}, & 60° < \delta \leq 180° \end{cases} \tag{13}$$

according to δ.

Therefore, when using the 3L2P configuration and assuming a maximum phase difference in $0 \leq \delta \leq 180°$, the voltage utilization is the same as that of the 4L2P configuration in $0 \leq \delta \leq 60°$. The utilization gradually decreases after 60°, and finally, at 180°, it reaches half of that in the 4L2P configuration. Therefore, the maximum efficiency interval in terms of voltage utilization is $0 \leq \delta \leq 60°$. Fig. 6 shows the pole voltages according to phase voltage at varying phase differences from 0° to 60° based on (7).

C. PROPOSED DPWM FOR 3L2P VSI

For three-leg three-phase (3L3P) VSIs, power loss reduction with DPWM was achieved in [15], [16]. The requirement of clamping time depends on the power factor of the load connected to the inverter output. Various types of DPWM have been proposed; for example, DPWMMIN and DPWMMAX for 120° clamping and DPWM1, DPWM2, and DPWM0 for 60° clamping, which reduce switching losses by unity, lagging, and leading power factors, respectively [17], [18]. In [19], 3L2P VSIs with DPWM were used to generate asymmetrical phase voltage outputs. However, these studies are applicable only to fixed phase differences. Hence, a study on the DPWM method considering a variable phase difference is required. Therefore, we propose a DPWM method for a sonar system.

The power factor of the load connected to the VSI is important for selecting DPWM modality, that is, DPWM1, DPWM2, or DPWM3. We focus on sonar transducers that have impedance matching circuits, and therefore, the power factor of the load can be assumed to be unity. The proposed DPWM method is thus based on DPWM1.

For operation of the 3L3P VSI with DPWM1, the pole voltage should be clamped to the DC rail in 60° intervals of each half cycle. Thus, the center of each DC-rail clamped segment is aligned with the cosine modulation wave peak. For example, the pole voltage is clamped to $V_{\rm dc}$ and $-V_{\rm dc}$ for 60° based on 0° and 180° (from −30° to 30° and from 150° to 210°, respectively), which are the points where the absolute value of V_{as} becomes the maximum. Thus, because the switch total losses are proportional to the switch conduction current [20], [21], it is advantageous in terms of switch losses compared with other clamping points where the switch conduction current is not the maximum. However, in the 3L2P configuration, because of the current superposition on the s phase current, there is a difference between the conventional DPWM1 and the DPWM method for 3L2P VSI in terms of centering the clamping position. The relation of each phase current is given by

$$i_s = -(i_a + i_b) \tag{14}$$

In (14), i_a, i_b, and i_s are a, b, and s phase currents, respectively. Therefore, if the phase voltage is equal to (6) and the voltage and current are unity, (14) can be rearranged as

$$i_s = -2I_m \cos(\delta) \cos\left(\omega_0 t + \frac{\delta}{2}\right) \tag{15}$$

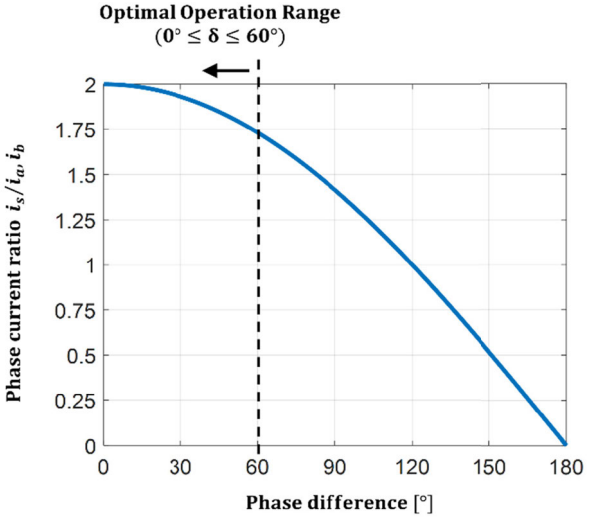

FIGURE 7. Phase current ratio according to phase difference δ.

In (15), I_m is the magnitude of the phase current. Therefore, assuming that I_m is constant, i_s is determined by the phase difference of i_a and i_b according to (15). Fig. 7 shows the ratio of i_s and other phase currents according to the phase difference when I_m is constant. Therefore, i_s is larger than other phase currents at 0° to 60°, which is the efficiency operation range in terms of voltage utilization induced (13). Therefore, the clamping point needs to be adjusted based on the point where the maximum current i_s occurs. According to (15), this point is placed at the middle of the maximum points of i_a and i_b ($\delta/2$); therefore, it should be selected considering the value of δ. Thus, even if the phase voltages and currents are unity, the clamping points cannot be selected as in the conventional DPWM1 method.

Pole voltages that have the maximum or minimum value in each leg have freedom for clamping to the DC rail (positive clamping or negative clamping); however, the pole voltage that has the middle value among the pole voltages cannot be clamped to the DC rail. In particular, V_{sN} can be clamped to the DC rail only if both V_{as} and V_{bs} are positive as shown in Fig. 8(a), or negative, as shown in Fig. 8(b). In other case, the V_{sN} has the middle value among the pole voltages; therefore, it cannot be clamped to DC rail. Assuming that V_{as} and V_{bs} references are cosine waveforms as in (6), V_{sN} can be clamped from −90°, which is the start angle for V_{as} to become positive, to 90° − δ, which is the start angle for V_{bs} to become negative. Therefore, intervals that can be clamped to the DC rail for V_{sN} may exist depending on the phase difference δ, and the intervals to maintain clamping decrease if the phase difference increases. For example, if δ is 0°, V_{sN} can be clamped to the DC rail at every moment because both V_{as} and V_{bs} have either positive or negative values at all time. In contrast, if δ is 180°, it cannot be clamped because both V_{as} and V_{bs} have opposite signs. Moreover, if δ exceed 120°, the interval where both V_{as} and V_{bs} are positive or negative values decrease to less than 60°. In other words, V_{sN} cannot be clamped to DC rail for 60°. Therefore, clamping intervals for each pole voltage cannot be equally divided for 60°. Thus, the switching loss of the leg responsible for V_{sN} at $\delta > 120°$ gradually increases, while the switching loss of the other legs gradually decreases, thereby resulting in an unbalanced switching loss of the legs. Therefore, the maximum available interval of the proposed DPWM is $0 < \delta < 120°$, which corresponds to the maximum angle to maintain 60° clamping. For clamping other pole voltages, two cases can be considered. If the sum of $V_{\rm max}$ and $V_{\rm min}$ is greater than zero, as shown in Fig. 8(c), $V_{\rm min}$ cannot be clamped to the DC rail due to constraint in (4). Thus, V_{sN} should be calculated such that $V_{\rm max}$ is clamped to the DC rail. In the second case, the sum of $V_{\rm max}$ and $V_{\rm min}$ is less than zero and V_{sN} should be calculated such that $V_{\rm min}$ is clamped to the DC rail, as shown in Fig. 8(d). Therefore, the conventional DPWM1 method can be modified by adding the phase difference as shown by the following equation

$$V_{sN} = \begin{cases} V_{\rm dc}, & 180° - \frac{\delta}{2} - \frac{\beta}{2} < \theta < 180° - \frac{\delta}{2} + \frac{\beta}{2} \\ -V_{\rm dc}, & -\frac{\delta}{2} - \frac{\beta}{2} < \theta < -\frac{\delta}{2} + \frac{\beta}{2} \\ V_{\rm dc} - V_{\rm max}, & V_{\rm max} + V_{\rm min} > 0 \\ -V_{\rm dc} - V_{\rm min}, & V_{\rm max} + V_{\rm min} < 0 \end{cases} \tag{16}$$

where $0° < \theta < 120°$ and the clamping interval is $\beta = 60°$. After determining V_{sN}, other pole voltages can be determined by (8).

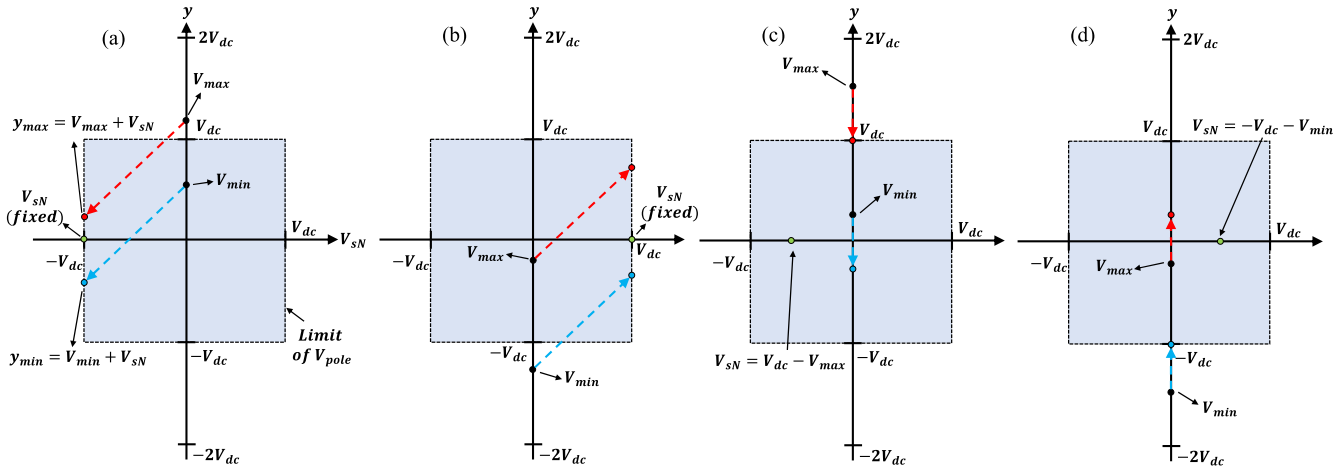

FIGURE 8. Pole voltage V_{sN} according to angle θ and phase voltage reference: (a) $-\delta/2 - \beta/2 < \theta < -\delta/2 + \beta/2$, (b) $\pi - \delta/2 - \beta/2 < \theta < \pi - \delta/2 + \beta/2$, (c) $V_{max} + V_{min} > 0$, and (d) $V_{max} + V_{min} < 0$.

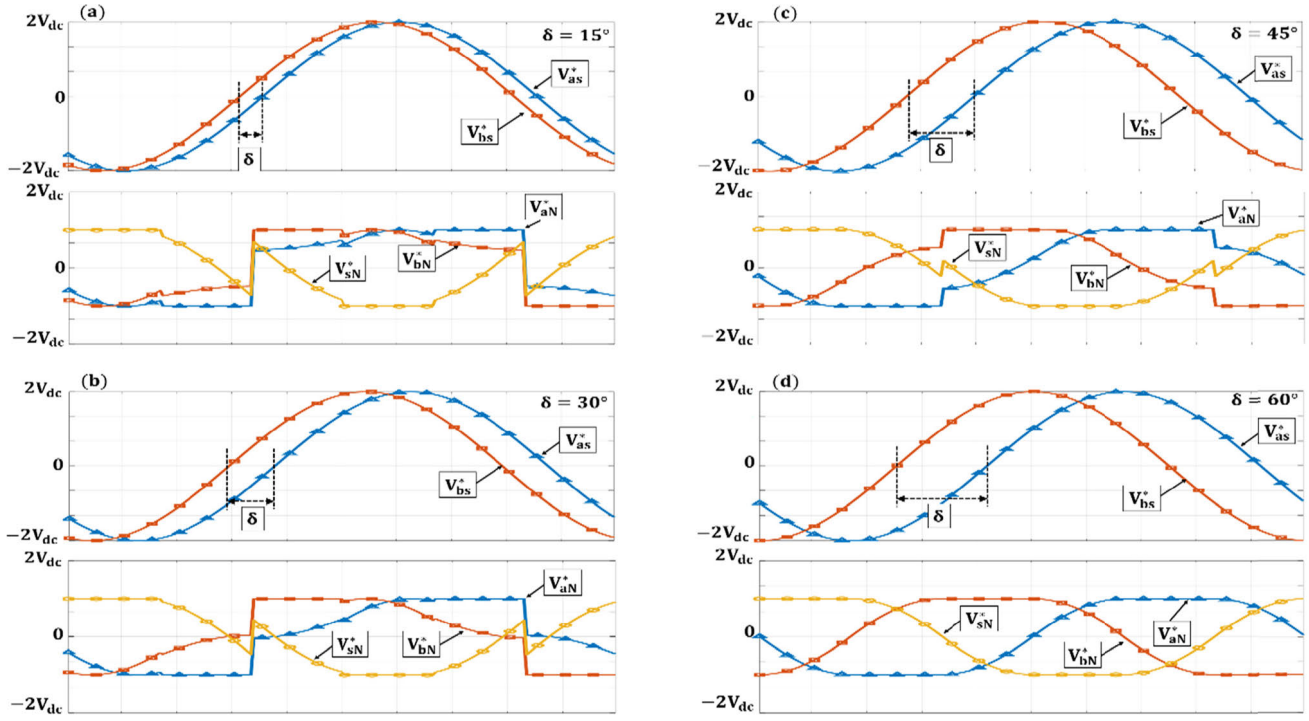

FIGURE 9. Phase voltage and pole voltage reference of DPWM according to phase difference ($V_m = 2V_{dc}$, $M = 1$): (a) $\delta = 15°$, (b) $\delta = 30°$, (c) $\delta = 45°$, and (d) $\delta = 60°$.

As the proposed DPWM method has the same constraints as those of the CPWM method, the magnitude of the maximum synthesizable phase voltage is determined using (13), which is similar to that for CPWM.

The maximum efficiency interval of the 3L2P configuration is determined using the voltage utilization and the operation method. Based on the small value, the maximum efficiency lies in $0 \leq \delta \leq 60°$. Fig. 9 shows the pole voltages according to the phase voltage at varying phase differences from 0° to 60°, based on (16).

III. TOTAL HARMONIC DISTORTION ANALYSIS

DPWM1 uses an effective switching frequency that is approximately two-thirds of the switching frequency f_{sw} for CPWM given the nonswitching interval. Thus, if the VSIs operate using DPWM and CPWM at the same switching frequency, the effective switching frequency falls under that in the case of CPWM when using DPWM, thereby reducing switching losses. However, switching losses can also be reduced by reducing the switching frequency of CPWM to match the effective switching frequency of DPWM. In this case, CPWM

generates similar switching losses as in the case of DPWM. The quality of VSI output voltage should be analyzed with respect to THD as it is affected by the MI and δ.

We analyze harmonic characteristics to determine the gain interval for the proposed DPWM compared with that for the conventional CPWM. For the theoretical analysis of harmonic characteristics, we derive a complete harmonic solution of phase voltage for each control technique and evaluate the normalized weighted total harmonic distortion (NWTHD) according to the output method. The NWTHD is given by

$$NWTHD = \frac{M}{V_1}\sqrt{\sum_{h=2}^{\infty}\left(\frac{V_h}{h}\right)^2} \tag{17}$$

where V_1 is the rms value of the fundamental component voltage, h is the order of harmonics, and V_h is the rms value of the h-th harmonic component [22]. This criterion is qualitatively equivalent to the factor introduced by Fukuda *et al.* [23] for determining harmonic distortion.

Bowes and Bird [24] compared the low-frequency waveform to be realized with a relatively high-frequency carrier waveform to determine the output value. If the carrier frequency ω_c and fundamental frequency ω_o are determined, when $x = \omega_c t$ and $y = \omega_o t$, a double-variable-controlled waveform $f(x, y)$ is given by

$$\begin{aligned} f(x,y) = \frac{A_{00}}{2} &+ \sum_{b=1}^{\infty}[A_{0b}\cos by + B_{0b}\sin by] \\ &+ \sum_{c=1}^{\infty}[A_{c0}\cos cx + B_{c0}\sin cx] \\ &+ \sum_{c=1}^{\infty}\sum_{\substack{b=-\infty \\ b\neq 0}}^{\infty}[A_{cb}\cos(cx+by) \\ &+ B_{cb}\sin(cx+by)] \end{aligned} \tag{18}$$

where

$$A_{cb} + jB_{cb} = \frac{1}{2\pi^2}\sum_i \int_{y_s(i)}^{y_e(i)}\int_{x_r(i)}^{x_f(i)} f(x,y)\, e^{j(cx+by)}\mathrm{d}x\,\mathrm{d}y \tag{19}$$

where c and b are the carrier and baseband index variables that define the frequency of each harmonic component of the phase leg output voltage. For example, if c and b are set to 2 and 4, respectively, it means that the fourth sideband harmonic in the group of harmonics is located around the second carrier harmonic. A_{cb} and B_{cb} are coefficients that represent the magnitude of the harmonic components for each c and b.

The first term in (18) represents the DC offset component of PWM waveform where $c = b = 0(A_{00})$. The second term corresponds to the output fundamental frequency waveform called baseband harmonics where $c = 0\ (x_{0b})$. The third term defines the carrier wave harmonics where $b = 0\ (x_{c0})$. The final double summation term, where $c, b \neq 0\ (x_{cb})$, is the ensemble of all possible frequencies between the carrier and baseband harmonics.

If we consider a continuous voltage reference waveform as in the sinusoidal PWM method, y_s and y_e are fixed at $-\pi$ and π, respectively. However, if the reference waveform is no longer continuous as in the proposed PWM method, we need to re-define the integral limits based on the change intervals of the voltage reference waveform. Thus, the outer and inner double Fourier integral limits, $y_s(i)$ and $y_e(i)$, are determined using (7) and (16). After determining $y_s(i)$ and $y_e(i)$, the rising and falling switching instants for each sector according to i—$x_r(i)$ and $x_f(i)$, respectively—are determined. Tables 2 and 3 list the integral limits for the conventional CPWM and proposed DPWM, respectively. Therefore, if the phase voltages for each control method are $V_{as,\mathrm{CPWM}}$, $V_{bs,\mathrm{CPWM}}$, $V_{as,\mathrm{DPWM}}$, and $V_{bs,\mathrm{DPWM}}$, then the complete harmonic solution can be expressed by (A.5)–(A.8) in the Appendix. To calculate (18), we set c and b from –10 to 10. As the Bessel function rapidly decreases beyond 10, it is reasonable to reduce the calculation time to achieve accuracy. The NWTHD of the phase voltage according to the MI and δ for each control method is shown in Fig. 10. In this case, the fundamental frequency, f_1, is set to 20 kHz, and the switching frequency of DPWM is 30 times the fundamental frequency, whereas the switching frequency of CPWM is 20 times the fundamental frequency, which is similar to the effective switching frequency of DPWM (two-thirds of the switching frequency). The NWTHD in the conventional CPWM increases as the MI and δ increase. In contrast, in the proposed DPWM, the NWTHD initially increases as that in CPWM; however, it decreases at a high MI (>0.6) and high δ, according to (18). Therefore, the superiority between CPWM and DPWM methods is determined in terms of the NWTHD according to the combination of the two variables, MI and δ. Based on the results, the superiority map is provided in Fig. 11. The MI increases in steps of 0.05 from 0.1 to 0.9, and the phase difference increases in steps of 10° from 0° to 120°. If the 3L2P VSIs operate at an MI and a δ of 0.8 and 60°, respectively, the proposed DPWM operating at a 600 kHz switching frequency is advantageous compared with the conventional CPWM operating at 400 kHz. If a switching frequency of 400 kHz is used for the CPWM, it is advantageous for the proposed DPWM to start at approximately 22°. Therefore, as the sonar system operates at fixed MI and δ during the emission of the acoustic signals, superior performance can be achieved by selecting the PWM according to the MI and δ. Fig. 12 shows the analytical and simulation results for the double-variable-controlled waveform.

IV. EXPERIMENTS AND RESULTS

A. EXPERIMENTAL SETUP

The following experiments were performed to verify the NWTHD superiority map of the conventional CPWM and proposed DPWM methods. The output voltage of the 3L2P VSI was measured, and the NWTHD was calculated using the fast Fourier transform implemented on MATLAB (MathWorks); the validity of the proposed map was then verified

TABLE 2. Outer and inner double fourier integral limits for CPWM.

i	Leg	$y_s(i)$	$y_e(i)$	$x_r(i)$	$x_f(i)$
1	A	$-\frac{3}{2}\pi$	$-\pi-\frac{\delta}{2}$	$-\frac{\pi}{2}[1+2M\cos y-M\cos(y+\delta)]$	$\frac{\pi}{2}[1+2M\cos y-M\cos(y+\delta)]$
	B			$-\frac{\pi}{2}[1+M\cos(y+\delta)]$	$\frac{\pi}{2}[1+M\cos(y+\delta)]$
	N			$-\frac{\pi}{2}[1-M\cos(y+\delta)]$	$\frac{\pi}{2}[1-M\cos(y+\delta)]$
2	A	$y_e(1)$	$-\frac{\pi}{2}-\delta$	$-\frac{\pi}{2}(1+M\cos y)$	$\frac{\pi}{2}(1+M\cos y)$
	B			$-\frac{\pi}{2}[1+2M\cos(y+\delta)-M\cos y]$	$\frac{\pi}{2}[1+2M\cos(y+\delta)-M\cos y]$
	N			$-\frac{\pi}{2}(1-M\cos y)$	$\frac{\pi}{2}(1-M\cos y)$
3	A	$y_e(2)$	$-\frac{\pi}{2}$	$-\frac{\pi}{2}[1+M\cos y-M\cos(y+\delta)]$	$\frac{\pi}{2}[1+M\cos y-M\cos(y+\delta)]$
	B			$-\frac{\pi}{2}[1-M\cos y+M\cos(y+\delta)]$	$\frac{\pi}{2}[1-M\cos y+M\cos(y+\delta)]$
	N			$-\frac{\pi}{2}[1-M\cos y-M\cos(y+\delta)]$	$\frac{\pi}{2}[1-M\cos y-M\cos(y+\delta)]$
4	A	$y_e(3)$	$-\frac{\delta}{2}$	$x_r(1)$	$x_f(1)$
	B				
	N				
5	A	$y_e(4)$	$\frac{\pi}{2}-\delta$	$x_r(2)$	$x_f(2)$
	B				
	N				
6	A	$y_e(5)$	$\frac{\pi}{2}$	$x_r(3)$	$x_f(3)$
	B				
	N				

TABLE 3. Outer and inner double fourier integral limits for DPWM.

i	Leg	$y_s(i)$	$y_e(i)$	$x_r(i)$	$x_f(i)$
1	A	$-\frac{7}{6}\pi-\frac{\delta}{2}$	$-\frac{5}{6}\pi-\frac{\delta}{2}$	$-\pi(1+M\cos y)$	$\pi(1+M\cos y)$
	B			$-\pi[1+M\cos(y+\delta)]$	$\pi[1+M\cos(y+\delta)]$
	N			$-\pi$	π
2	A	$y_e(1)$	$-\frac{\pi}{2}-\frac{\delta}{2}$	0	0
	B			$-\pi[M\cos y+M\cos(y+\delta)]$	$\pi[M\cos y+M\cos(y+\delta)]$
	N			$\pi M\cos y$	$-\pi M\cos y$
3	A	$y_e(2)$	$-\frac{\pi}{6}-\frac{\delta}{2}$	$-\pi[1+M\cos y-M\cos(y+\delta)]$	$\pi[1+M\cos y-M\cos(y+\delta)]$
	B			$-\pi$	π
	N			$-\pi[1-M\cos(y+\delta)]$	$\pi[1-M\cos(y+\delta)]$
4	A	$y_e(3)$	$-\frac{\delta}{2}+\frac{\pi}{6}$	$-\pi M\cos y$	$\pi M\cos y$
	B			$-\pi M\cos(y+\delta)$	$\pi M\cos(y+\delta)$
	N			0	0
5	A	$y_e(4)$	$\frac{\pi}{2}-\frac{\delta}{2}$	$-\pi$	π
	B			$-\pi[1-M\cos y+M\cos(y+\delta)]$	$\pi[1-M\cos y+M\cos(y+\delta)]$
	N			$-\pi(1-M\cos y)$	$\pi(1-M\cos y)$
6	A	$y_e(5)$	$\frac{5}{6}\pi-\frac{\delta}{2}$	$-\pi[M\cos y-M\cos(y+\delta)]$	$\pi[M\cos y-M\cos(y+\delta)]$
	B			0	0
	N			$\pi M\cos(y+\delta)$	$-\pi M\cos(y+\delta)$

by comparing the mathematical analysis and experimental results. In addition, although the proposed method is advantageous in terms of the NWTHD, it cannot be applied when the switch losses increase, phase difference control is not possible, or voltage utilization decreases. Therefore, under the same load conditions, the heat sink temperature, phase

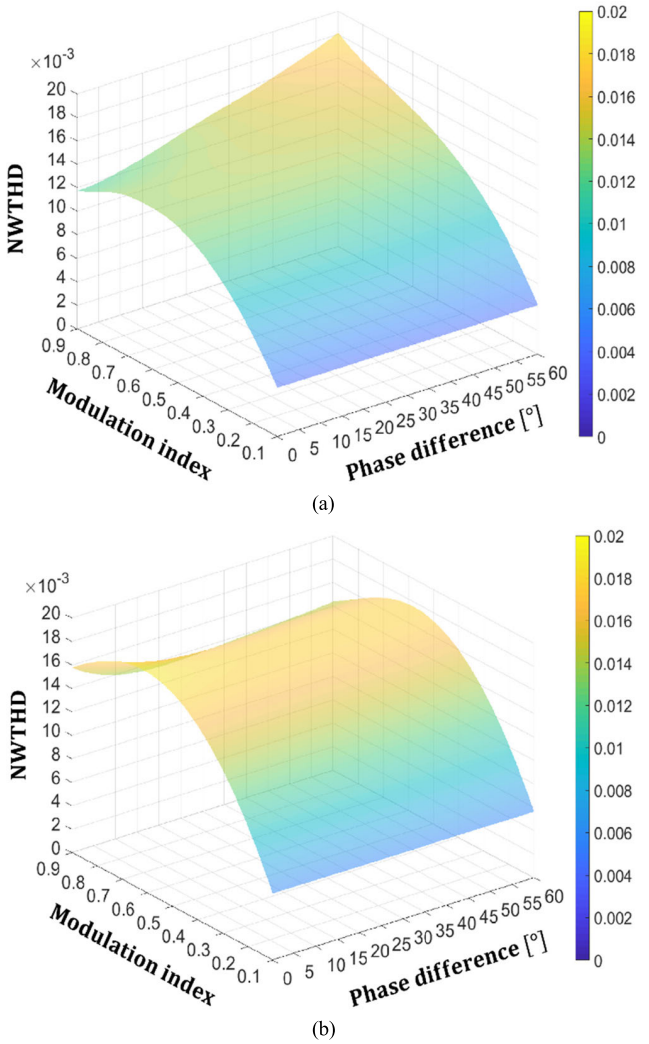

FIGURE 10. NWTHD (analytical result) for (a) CPWM at $f_{sw} = 400$ kHz and (b) DPWM at $f_{sw} = 600$ kHz.

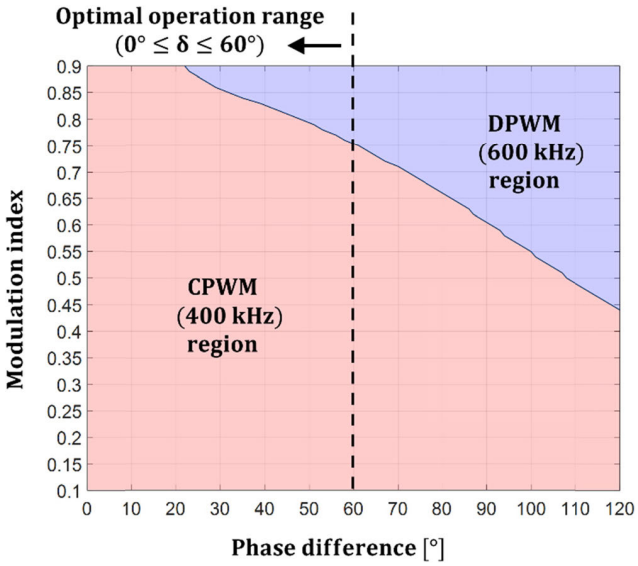

FIGURE 11. Optimal PWM extraction according to MI and phase difference.

TABLE 4. System parameters.

Parameter	Value
DC link voltage ($2V_{dc}$)	150 V
Fundamental frequency	20 kHz
Low-pass filter inductance	120 μH
Low-pass filter capacitance	120 pF
Low-pass filter cut-off frequency	125 kHz
Transformer magnetizing inductance	260 μH
Transformer turn ratio	5
Load impedance magnitude @ 20 kHz	398.6 Ω
Load impedance phase @ 20 kHz	−2.1°

difference control ability, and voltage utilization were measured to verify the similarity of important evaluation factors for sonar systems.

For our experiment, we considered system parameters as summarized in Table 4. The switching frequency was set to 600 kHz for DPWM and 400 kHz for CPWM, and the phase difference varied in increments of 10° between 0° and 60°, which corresponds to the maximum efficiency range of the 3L2P configuration in terms of voltage utilization. Further, the MI was varied in increments of 0.1 between 0.3 and 0.9. All experiments were performed under the same load conditions. Fig. 13 shows the experimental setup, which comprises a module that connects one impedance matching transformer to each sonar equivalent model. A total of five modules are connected in series to create a set that is combined with a lowpass filter to constitute the total load. The load is then connected to the VSI to complete the sonar transducer power system. The impedance magnitude and phase of the total load are 398.6 Ω and −2.1°, respectively. Therefore, the total load can be regarded as unity. The experimental configuration consists of a control board implemented by the 32-bit TMS320C28346 manufactured by Texas Instruments.

B. NWTHD MEASUREMENT RESULTS

To compare the NWTHD between the modulation methods, we measured the 3L2P VSI output voltage, as shown in Fig. 14 and Fig. 15. Based on the above results, the NWTHD of the CPWM method gradually increased as the MI and δ increased, whereas the NWTHD of the DPWM method has similar characteristics to that in CPWM up to an MI of 0.6. After the MI of 0.6, the NWTHD decreases, resulting in a marked difference than in CPWM, as shown Fig. 16. These characteristics are the same as the results of the mathematical analysis presented in Section III. The average

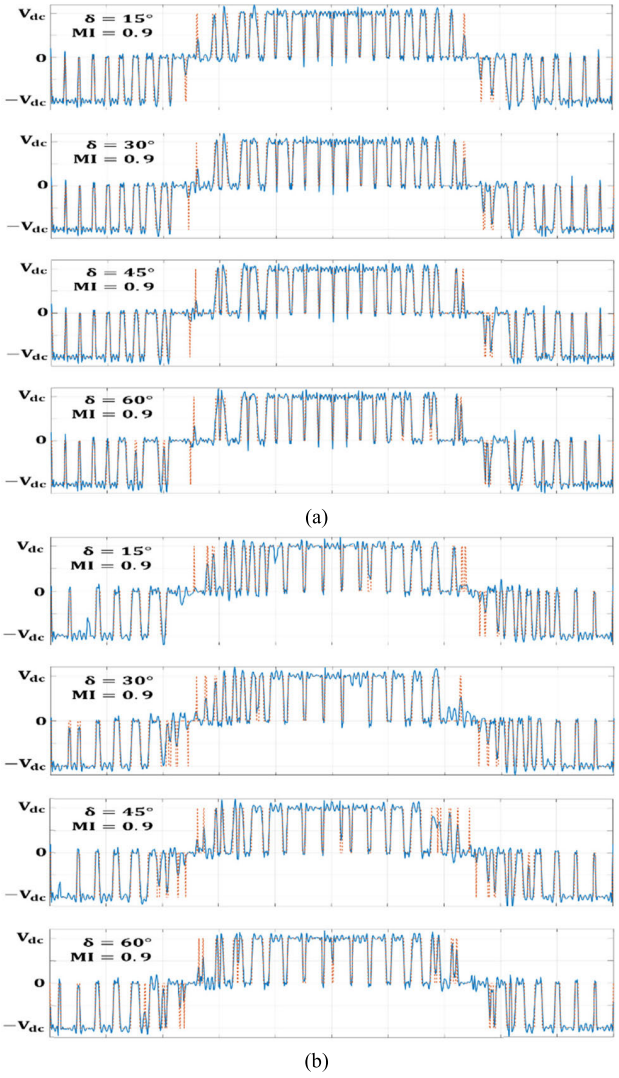

FIGURE 12. Analytical results of double-variable-controlled waveform compared to simulation results: (a) conventional CPWM at $f_{sw} = 400$ kHz (solid line: analytical result; dashed line: simulation result) and (b) proposed DPWM $f_{sw} = 600$ kHz (solid line: analytical result; dashed line: simulation result).

errors between the analytical and experimental values for the CPWM and DPWM methods are 2.4% and 1.9%, respectively. These errors are caused by nonideal factors, such as rising time, falling time, and dead time of the VSI output waveform, in the actual experiment. In this experiment, SiC MOSFET manufactured by ROHM was used, and the dead time was set at 70 *ns*. This dead time corresponds to 4% of one cycle ($\approx$1.67 μs) based on a switching frequency of 600 *kHz*. The dead time is expressed as a decrease in MI compared with the MI set according to the inverter output voltage reference, which can increase the NWTHD error. Further, in this study, the dead time compensation method was not used, and only the pure PWM method was compared. There errors occur because the PWM is achieved using a regular sampling method in a practical scenario, whereas the

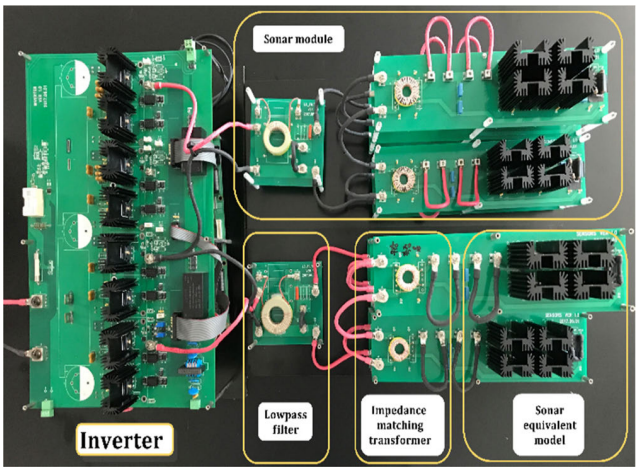

FIGURE 13. Experimental setup to evaluate VSI and proposed DPWM.

mathematical analysis in our study considered the natural sampling method. However, the average error is below 2.5%, which is sufficiently small to validate the real system. Therefore, the complete harmonic solution derived from this study is effective for deriving an advantageous method in terms of the NWTHD between the conventional CPWM and proposed DPWM methods based on the MI and phase differences. Fig.17 shows the superiority map of CPWM and DPWM methods according to the experimental results.

C. HEAT SINK TEMPERATURE MEASUREMENT RESULTS

Even if it is excellent in terms of the NWTHD, a significant degradation in terms of switching losses causes an increase in the volume because of the increase in the heat sink area. Therefore, we measured the heat sink temperature to verify whether the switching losses of the CPWM and DPWM are similar. An MI of 0.9 was applied, and the initial and steady temperatures were measured using an infrared thermometer. In this case, it is important to choose the emissivity from a material in the measurement target to obtain accurate results. In this study, we selected anodized aluminum as the target material with emissivity set from 0.8 to 0.82 according to the heat sink temperature during measurements [25]. Fig. 18 shows the temperature of the heat sink according to the phase difference, where S_{xH} denotes the upper switch of the x leg. The average temperature increase (ΔT) of CPWM and DPWM was 29.0 and 30.5 °C, respectively, with a difference of 1.5 °C that represents approximately 5.25% of the average temperature increase than in the case of CPWM. Therefore, the two methods are similar in terms of switching loss, which suggests the feasibility to apply both CPWM and DPWM with the same heat sink.

D. VOLTAGE UTILIZATION AND PHASE DIFFERENCE MEASUREMENT RESULTS

In addition to switching losses, voltage utilization and phase difference control ability were verified through experiments.

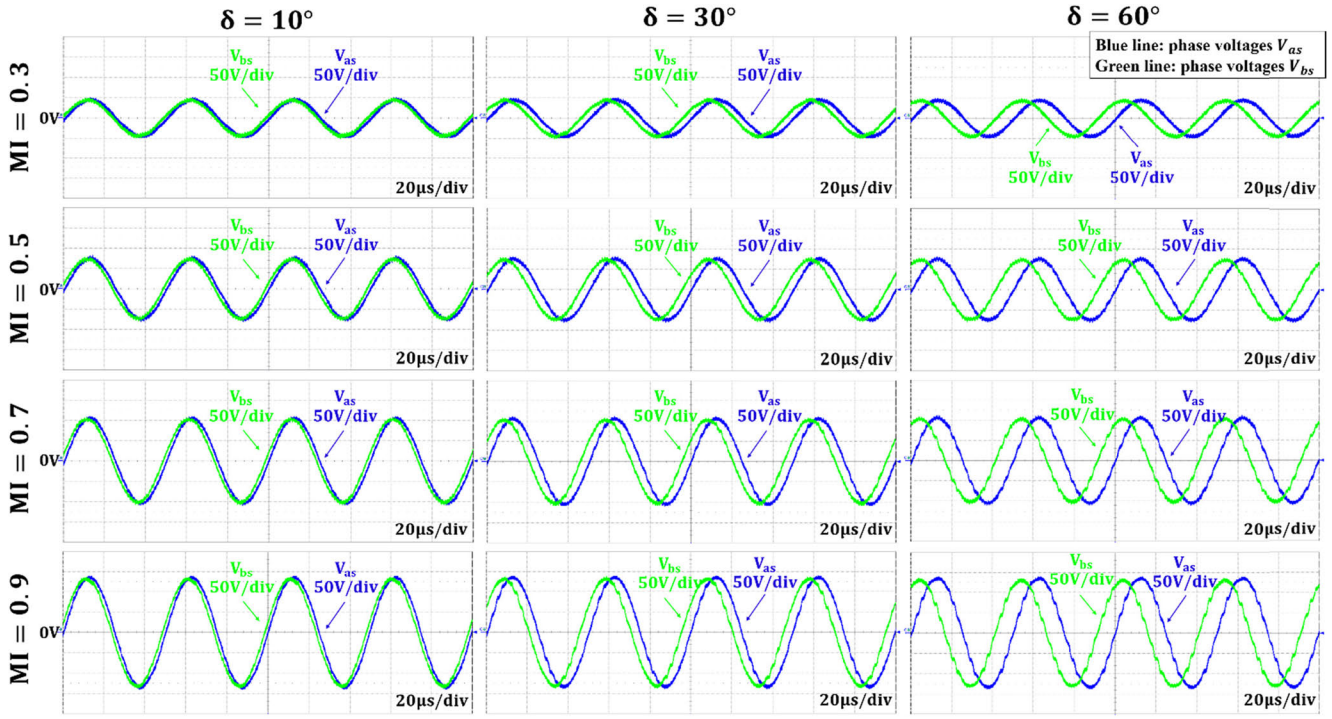

FIGURE 14. Phase voltage of 3L2P VSI (filtered waveform by lowpass filter) using CPWM.

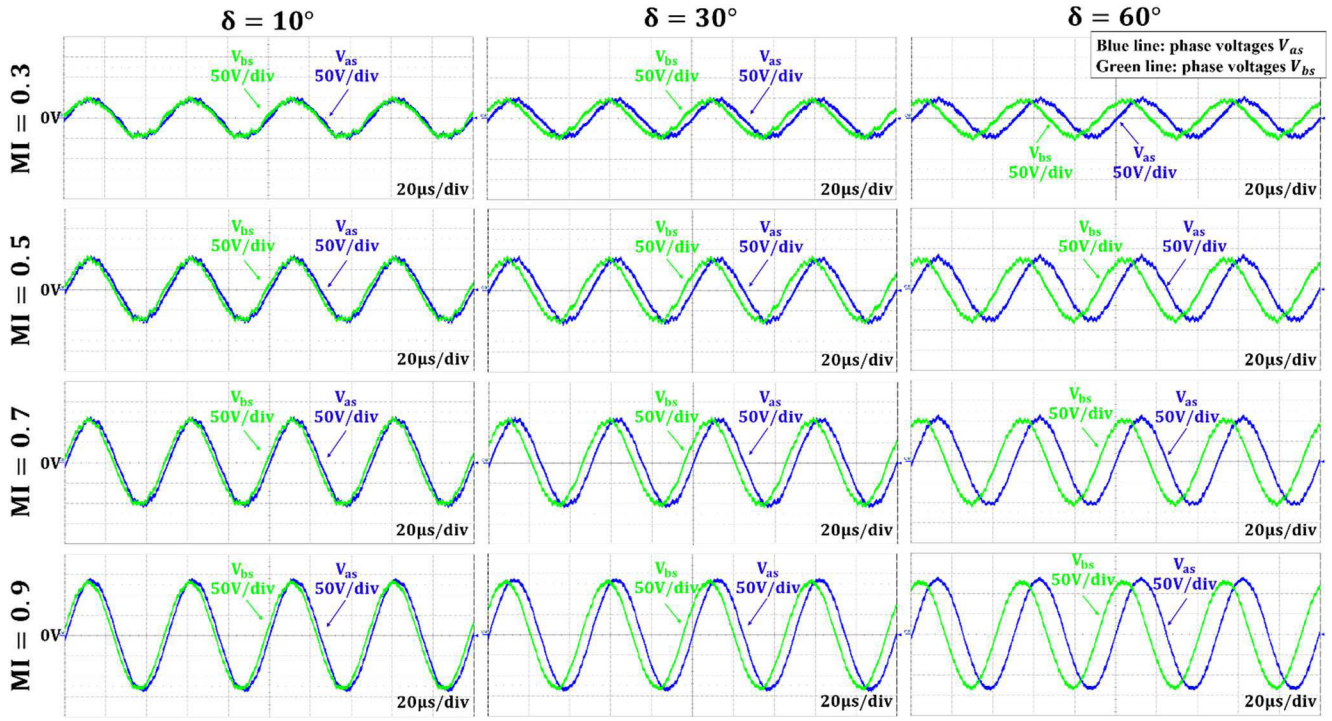

FIGURE 15. Phase voltage of 3L2P VSI (filtered waveform by lowpass filter) using DPWM.

To confirm the phase difference, the 3L2P VSI voltage outputs were measured, and the fundamental component was obtained using the Fourier transform in MATLAB. Thereafter, the measured values of the reference were compared and verified. For verifying voltage utilization, the input voltage of the sonar equivalent model, which was lowpass

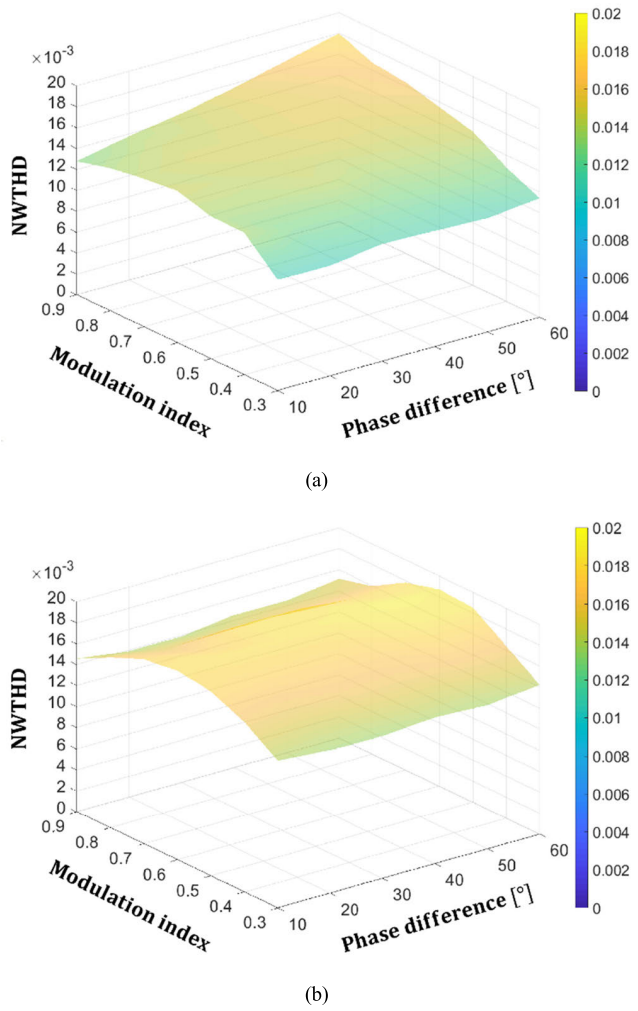

FIGURE 16. NWTHD (experimental result) for (a) CPWM and (b) DPWM.

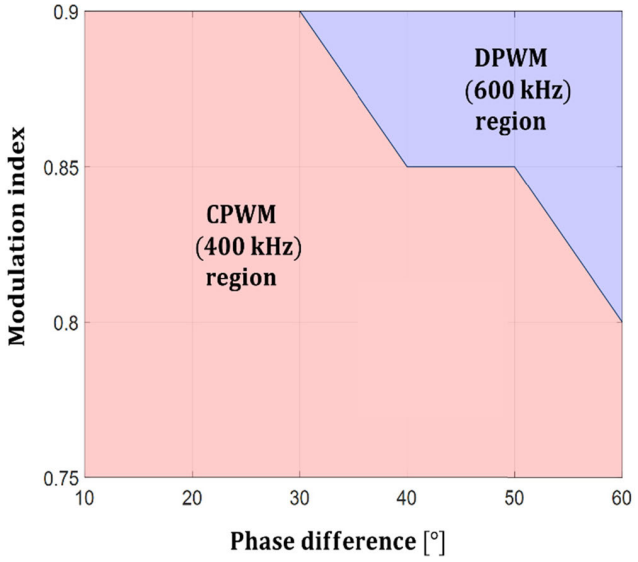

FIGURE 17. Optimal PWM extracted by experimental results.

filtered, was measured as shown in Fig. 14 and 15; then, the rms value was directly obtained from a function on an oscilloscope. Tables 5 and 6 list the results for the phase difference between CPWM and DPWM, respectively. The mean error of CPWM is 0.4°, which is equal to that of DPWM. Thus, both methods enable variable phase differences. Table 7 lists the input voltage of the sonar equivalent circuit measured under the 0-dB gain of the lowpass filter for the fundamental frequency and all other harmonics below −30 dB, compared with the magnitude of the fundamental frequency. In addition, the MI was set to 0.9, and the output voltage reference was 95.5 V_{rms} ($2V_{dc}MI/\sqrt{2}$), which corresponds to the voltage utilization of the 4L2P VSI. The mean values of CPWM and DPWM are 96.2 and 96.8 V_{rms}. Compared with the reference, the errors are 0.8% and 1.4%, respectively. Therefore, it was verified that both methods showed similar characteristics in terms of voltage utilization and phase difference variability.

E. RESULT DISCUSSION

We provided the guidelines for the selection of the PWM method to improve the output voltage quality in terms of the NWTHD. If MIs are set at 0.8–0.9 in increments of 0.05 and δ values set at 10–60° in increments of 10° (assuming that the operating times for the points are the same), the average NWTHD is 1.52% when CPWM alone is used. However, when the PWM method is selected according to the guidelines, the average NWTHD is 1.46%, which is 96% of that in the case where only CPWM is used; therefore, there is a reduction of 4%. However, as the minimum value of the set MI increases, the effect of the proposed method increases. Therefore, when the MI is fixed at 0.9, the average NWTHD is 1.52% for the conventional CPWM method and 1.41% for the proposed DPWM method, which is 92.5% of that for the conventional CPWM method; thus, a high reduction of 7.5% can be expected. However, if the MI is below 0.75, PWM selection is meaningless because the NTWHD reverses at this point. This paper is significant in that it suggests the correct selection criteria by creating the superiority map based on mathematical analysis. In addition, through the experiment, it is verified that the average error between the analyzed and experimental values is approximately 2.2%, which is meaningful in practical application. This reduces the time and cost required to create a superiority map by measuring the NWTHD through repeated experiments.

The results of the heat sink temperature measurement confirmed that the ΔT of the CPWM and DWPM methods were 29.0 and 30.5 °C, respectively. The results of the phase difference experiment confirmed that phase differences within a mean error of 0.4° can be realized for both the methods. For voltage utilization, we analyzed the sonar sensor input voltage. The experimental results confirm that the voltage error compared with the voltage reference was similar to those of CPWM and DPWM, (0.8% and 1.4%, respectively). As a result, it is verified that the characteristics (except the NWTHD) are similar in both CPWM and DPWM methods. This means that it is not required to change the hardware,

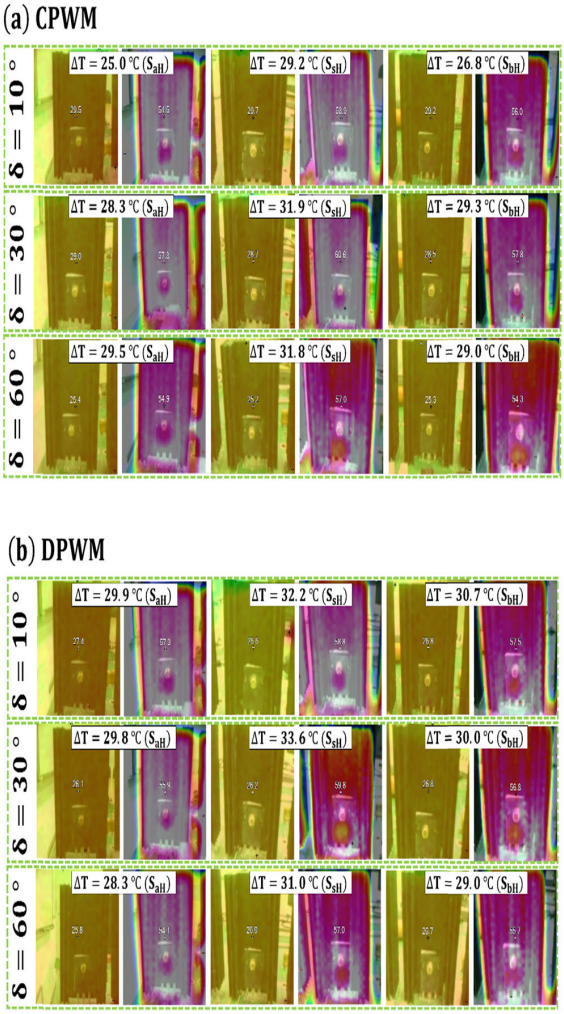

FIGURE 18. Heat sink temperature measurements ($MI = 0.9$) for (a) CPWM and (b) DPWM.

TABLE 5. Phase difference measurement results for CPWM.

Phase difference reference (°)	CPWM (°)			
	MI 0.75	MI 0.8	MI 0.85	MI 0.9
10	10.2	10.2	10.2	10.1
20	20.2	20.2	20.3	20.4
30	30.2	30.6	30.5	30.3
40	40.5	40.6	40.4	40.5
50	50.7	50.5	50.5	50.6
60	60.5	60.7	60.6	60.4

such as the heat sink of the inverter, to apply the proposed DPWM method. Therefore, by selecting the PWM method according to the proposed guidelines, the NWTHD can be reduced without changing the hardware.

TABLE 6. Phase difference measurement results for DPWM.

Phase difference reference (°)	CPWM (°)			
	MI 0.75	MI 0.8	MI 0.85	MI 0.9
10	10.0	10.0	10.2	10.3
20	20.4	20.4	20.4	20.5
30	30.3	30.5	30.4	30.3
40	40.5	40.6	40.5	40.5
50	50.6	50.6	50.5	50.6
60	60.8	60.5	60.7	60.5

TABLE 7. Input voltage of sonar equivalent circuit.

Phase difference (°)	CPWM		DPWM	
	Phase A (V_{rms})	Phase B (V_{rms})	Phase A (V_{rms})	Phase B (V_{rms})
10	95.3	97.1	96.4	97.6
20	95.1	97.1	95.6	97.5
30	95.2	97.2	95.6	97.4
40	95.1	97.3	96.0	97.8
50	94.9	97.3	95.7	97.9
60	95.5	97.6	95.9	97.9
Mean value	95.2	97.3	95.9	97.7

Moreover, our proposed method reduced the THD in the output voltage of 3L2P VSI. Therefore, if the 3L2P structure is used, it can be extended not only to the sonar system but also to any type of load directly without modification.

V. CONCLUSION

We proposed a DPWM method to drive the 3L2P VSI of a sonar system. If the sonar system is operated by selecting the advantageous method in terms of the NWTHD among the conventional CPWM and proposed DPWM methods based on the proposed superiority map, the sonar systems can be operated to achieve the NWTHD characteristics without deteriorating the characteristics of switching losses, phase difference variability, and voltage utilization. However, since the THD reduction is determined according to the range of the MI, the proposed method may be meaningless when the

MI is below a certain level. Also, in the proposed DPWM, we assumed that the conduction loss was very small compared with the switching loss owing to the small load. Consequently, we neglected the conduction loss and reduced the switching loss. Nevertheless, when the load increases due to the characteristics of the 3L2P configuration, current concentrates in the common leg depending on the phase difference, which increases the conduction loss of the common leg switches. Therefore, in future research, we plan to investigate the distribution of the nonswitching interval, considering both the switching loss and conduction loss due to phase difference.

$$
\begin{aligned}
A_{cb}+jB_{cb} = {} & \frac{2V_{\mathrm{dc}}}{c\pi^2}\sum_{k=-\infty}^{\infty}\Bigg[\frac{2}{[k+b]}J_k\left(cM\pi\right)\sin\left([k+b]\,\frac{\pi}{6}\right)\Bigg\{\left(2\cos\left(k\frac{\delta}{2}+[k+b]\,\frac{2\pi}{3}\right)+\mathrm{e}^{-j\frac{1}{2}k\delta}\right)\times\sin\left(k\frac{\pi}{2}\right)\mathrm{e}^{-j\frac{1}{2}b\delta} \\
& +2\cos\left(k\frac{\delta}{2}+[k+b]\,\frac{\pi}{3}\right)\sin\left([k-2c]\,\frac{\pi}{2}\right)\mathrm{e}^{-j\frac{1}{2}b\delta}+\sin\left(k\frac{\pi}{2}+c\pi\right)\mathrm{e}^{-j\frac{1}{2}[k+b][\delta+2\pi]}\Bigg\}\Bigg|_{k\neq-b} \\
& +\frac{2\pi}{j3}J_k\left(cM\pi\right)\cos\left(c\frac{\pi}{2}\right)\sin\left(k\frac{\pi}{2}\right)\left\{j3\cos\left(k\frac{\delta}{2}\right)+\sin\left(k\frac{\delta}{2}\right)\right\}\mathrm{e}^{j\frac{1}{2}(k\delta+3c\pi)}\Bigg|_{k=-b}\Bigg] \\
& +\frac{2V_{\mathrm{dc}}}{c\pi^2}\sum_{k=-\infty}^{\infty}\sum_{h=-\infty}^{\infty}\Bigg[-\frac{2}{j[h+k+b]}J_h\left(cM\pi\right)\times J_k\left(cM\pi\right)\sin\left([h+k+b]\,\frac{\pi}{6}\right) \\
& \times\Bigg\{j\sin\left([\mathrm{h\text{-}k}]\,\frac{\pi}{2}\right)\mathrm{e}^{j\frac{1}{6}(3[h-\mathrm{k\text{-}b}]\delta+4[h+k+b]\pi)}-\sin\left([h-k-2c]\,\frac{\pi}{2}\right) \\
& \times\mathrm{e}^{-j\frac{1}{6}(3[-h+k+b]\delta+3\pi+2[h+k+b]\pi)}\Bigg\}\Bigg|_{k+h\neq-b}-\frac{2\pi}{3}\mathrm{e}^{jh\delta}J_h\left(cM\pi\right)J_k\left(cM\pi\right)\cos\left(c\frac{\pi}{2}\right) \\
& \times\sin\left([h-\mathrm{k\text{-}c}]\,\frac{\pi}{2}\right)\Bigg|_{k+h=-b}\Bigg]
\end{aligned}
\tag{A.4}
$$

$$
V_{\mathrm{as,DPWM}} = 2MV_{\mathrm{dc}}\cos y+\sum_{c=1}^{\infty}\sum_{b=-\infty}^{\infty}\left[A_{\mathrm{ad}}\cos\left(cx+by\right)+B_{\mathrm{ad}}\sin\left(cx+by\right)\right]
$$

$$
\begin{aligned}
A_{\mathrm{ad}}+jB_{\mathrm{ad}} = {} & \frac{2V_{\mathrm{dc}}}{c\pi^2}\sum_{k=-\infty}^{\infty}\Bigg[\frac{2}{[k+b]}J_k\left(cM\pi\right)\sin\left([k+b]\,\frac{\pi}{6}\right)\times\Bigg\{\left(2\cos\left(k\frac{\delta}{2}+[k+b]\,\frac{2\pi}{3}\right)+\mathrm{e}^{-j\frac{1}{2}k\delta}\right)\sin\left(k\frac{\pi}{2}\right)\mathrm{e}^{-j\frac{1}{2}b\delta} \\
& +2\cos\left(k\frac{\delta}{2}+[k+b]\,\frac{\pi}{3}\right)\sin\left([k-2c]\,\frac{\pi}{2}\right)\mathrm{e}^{-j\frac{1}{2}b\delta}+\sin\left(k\frac{\pi}{2}+c\pi\right)\mathrm{e}^{-j\frac{1}{2}[k+b][\delta+2\pi]}\Bigg\}\Bigg|_{k\neq-b} \\
& +\frac{2\pi}{j3}J_k\left(cM\pi\right)\cos\left(c\frac{\pi}{2}\right)\sin\left(k\frac{\pi}{2}\right)\left\{j3\cos\left(k\frac{\delta}{2}\right)+\sin\left(k\frac{\delta}{2}\right)\right\}\mathrm{e}^{j\frac{1}{2}(k\delta+3c\pi)}\Bigg|_{k=-b}\Bigg] \\
& +\frac{2V_{\mathrm{dc}}}{c\pi^2}\sum_{k=-\infty}^{\infty}\sum_{h=-\infty}^{\infty}\Bigg[-\frac{2}{j[h+k+b]}J_h\left(cM\pi\right)J_k\left(cM\pi\right)\sin\left([h+k+b]\,\frac{\pi}{6}\right) \\
& \times\Bigg\{j\sin\left([h-k]\,\frac{\pi}{2}\right)\mathrm{e}^{j\frac{1}{6}(3[h-\mathrm{k\text{-}b}]\delta+4[h+k+b]\pi)}-\sin\left([h-k-2c]\,\frac{\pi}{2}\right)\mathrm{e}^{-j\frac{1}{6}(3[-h+k+b]\delta+3\pi+2[h+k+b]\pi)}\Bigg\}\Bigg|_{k+h\neq-b} \\
& -\frac{2\pi}{3}\mathrm{e}^{jh\delta}J_h\left(cM\pi\right)J_k\left(cM\pi\right)\cos\left(c\frac{\pi}{2}\right)\sin\left([h-\mathrm{k\text{-}c}]\,\frac{\pi}{2}\right)\Bigg|_{k+h=-b}\Bigg]
\end{aligned}
\tag{A.5}
$$

$$
V_{\mathrm{bs,DPWM}} = 2MV_{\mathrm{dc}}\cos\left(y+\delta\right)+\sum_{c=1}^{\infty}\sum_{b=-\infty}^{\infty}\left[A_{\mathrm{bd}}\cos\left(cx+by\right)+B_{\mathrm{bd}}\sin\left(cx+by\right)\right]
$$

$$
\begin{aligned}
A_{\mathrm{bd}}+jB_{\mathrm{bd}} = {} & \frac{2V_{\mathrm{dc}}}{c\pi^2}\sum_{k=-\infty}^{\infty}\Bigg[\frac{2}{j[k+b]}J_k\left(cM\pi\right)\sin\left([k+b]\,\frac{\pi}{6}\right)\times\Bigg\{j\left(2\cos\left(k\frac{\delta}{2}+[k+b]\,\frac{2\pi}{3}\right)+\mathrm{e}^{j\frac{1}{2}k\delta}\right)\sin\left(k\frac{\pi}{2}\right)\mathrm{e}^{-j\frac{1}{2}b\delta} \\
& +j2\cos\left(k\frac{\delta}{2}-[k+b]\,\frac{\pi}{3}\right)\sin\left([k-2c]\,\frac{\pi}{2}\right)\mathrm{e}^{-\frac{1}{2}jb\delta}-\sin\left(k\frac{\pi}{2}+c\pi\right)\mathrm{e}^{-j\frac{1}{2}([-k+b]\delta+\pi+2[k+b]\pi)}\Bigg\}\Bigg|_{k\neq-b} \\
& +\frac{2\pi}{3}J_k\left(cM\pi\right)\cos\left(c\frac{\pi}{2}\right)^2\sin\left(k\frac{\pi}{2}\right)\left(1+2\mathrm{e}^{jk\delta}\right)\Bigg|_{k=-b}\Bigg] \\
& +\frac{2V_{\mathrm{dc}}}{c\pi^2}\sum_{k=-\infty}^{\infty}\sum_{h=-\infty}^{\infty}\Bigg[-\frac{2}{j[h+k+b]}J_h\left(cM\pi\right)J_k\left(cM\pi\right)\sin\left([h+k+b]\,\frac{\pi}{6}\right) \\
& \times\Bigg\{\sin\left([h-k]\,\frac{\pi}{2}\right)\mathrm{e}^{-j\frac{1}{6}(3[-h+k+b]\delta+3\pi+4[h+k+b]\pi)}-j\sin\left([h-k+2c]\,\frac{\pi}{2}\right)\mathrm{e}^{j\frac{1}{6}(3[h-\mathrm{k\text{-}b}]\delta+2[h+k+b]\pi)}\Bigg\}\Bigg|_{k+h\neq-b} \\
& +\frac{2\pi}{3}\mathrm{e}^{j\delta h}J_h\left(cM\pi\right)J_k\left(cM\pi\right)\cos\left(c\frac{\pi}{2}\right)\sin\left([h-k+c]\,\frac{\pi}{2}\right)\Bigg|_{k+h=-b}\Bigg]
\end{aligned}
\tag{A.6}
$$

As sonar systems are essential for the Agency for Defense Development and thus national security, the proposed method, which aims to increase the detection accuracy of such systems, will contribute to enhanced security

APPENDIX

The relationship between the phase voltage and pole voltage of 3L2P is expressed using (1). Therefore, harmonic solution of the phase voltage is obtained by determining the difference between each pole voltage harmonic solution after deriving the harmonic solutions for the pole voltages. Therefore, general form of the Fourier integral given by (19) must be solved for determining the coefficients of each pole voltage. To derive the coefficient V_{as} for proposed DPWM method, following cases should be considered. First, when both the carrier index variable c and baseband index variable b are zero; second, c is zero and b is non-zero; third, c is greater than zero and b is zero; and fourth, c is greater than zero and b is non-zero. The first case represents the DC offset component. The second case corresponds to the

$$
\begin{aligned}
V_{\mathrm{as,CPWM}} &= 2MV_{\mathrm{dc}}\cos y + \sum_{c=1}^{\infty}\sum_{b=-\infty}^{\infty}\left[A_{\mathrm{ac}}\cos\left(cx+by\right)+B_{\mathrm{ac}}\sin\left(cx+by\right)\right] \\
A_{\mathrm{ac}}+jB_{\mathrm{ac}} &= \frac{2V_{\mathrm{dc}}}{c\pi^2}\sum_{k=-\infty}^{\infty}\Bigg[\frac{4}{[k+b]}J_k\left(c\frac{M}{2}\pi\right)\cos\left([k+b]\frac{\pi}{2}\right)\times\Bigg\{\sin\left([\mathrm{k\text{-}c}]\frac{\pi}{2}\right)\Bigg[\sin\left(k\frac{\delta}{2}\right)-\sin\left([2k+b]\frac{\delta}{2}\right. \\
&\quad \left.-\sin\left([k+b]\frac{\pi}{2}\right)\right)\Bigg]\mathrm{e}^{-j\frac{1}{2}(b\delta+[k+b]\pi)}-\sin\left([k+b]\frac{\delta-\pi}{4}\right)\sin\left([k+c]\frac{\pi}{2}\right)\mathrm{e}^{-j\frac{1}{4}[k+b][3\delta+\pi]}\Bigg\}\Bigg|_{k\neq-b} \\
&\quad +\left(-\delta+\pi\right)J_k\left(c\frac{M}{2}\pi\right)\left\{\sin\left([\mathrm{k\text{-}c}]\frac{\pi}{2}\right)\left(1+\mathrm{e}^{jk\delta}\right)+\sin\left([k+c]\frac{\pi}{2}\right)\right\}\Bigg|_{k=-b}\Bigg] \\
&\quad +\frac{2V_{\mathrm{dc}}}{c\pi^2}\sum_{k=-\infty}^{\infty}\sum_{h=-\infty}^{\infty}\Bigg[-\frac{4}{j\left[h+k+b\right]}J_h\left(c\frac{M}{2}\pi\right)\cos\left([h+k+b]\frac{\pi}{2}\right) \\
&\quad \times\Bigg\{J_k\left(cM\pi\right)\sin\left([h-\mathrm{k\text{-}c}]\frac{\pi}{2}\right)\sin\left([h+k+b]\frac{\delta-\pi}{4}\right)\mathrm{e}^{-j\frac{1}{4}([-3h+k+b]\delta+2\pi+3[h+k+b]\pi)} \\
&\quad +2J_k\left(c\frac{M}{2}\pi\right)\cos\left([\mathrm{h\text{-}c}]\frac{\pi}{2}\right)\sin\left([h+k+b]\frac{\delta-\pi}{2}\right)\sin\left(k\frac{\pi}{2}\right)\mathrm{e}^{-j\frac{1}{2}([-h+k+b]\delta+[1+h+k+b]\pi)}\Bigg\}\Bigg|_{k+h\neq-b} \\
&\quad +\mathrm{e}^{jh\delta}J_h\left(c\frac{M}{2}\pi\right)\left\{\left(\delta-\pi\right)J_k\left(cM\pi\right)\sin\left([h-k-c]\frac{\pi}{2}\right)+4\delta J_k\left(c\frac{M}{2}\pi\right)\cos\left([h-c]\frac{\pi}{2}\right)\sin\left(k\frac{\pi}{2}\right)\right\}\Bigg|_{k+h=-b}\Bigg]
\end{aligned}
\tag{A.7}
$$

$$
\begin{aligned}
V_{\mathrm{bs,CPWM}} &= 2MV_{\mathrm{dc}}\cos(y+\delta) + \sum_{c=1}^{\infty}\sum_{b=-\infty}^{\infty}\left[A_{\mathrm{bc}}\cos\left(cx+by\right)+B_{bc}\sin\left(cx+by\right)\right] \\
A_{\mathrm{bc}}+jB_{\mathrm{bc}} &= \frac{2V_{\mathrm{dc}}}{c\pi^2}\sum_{k=-\infty}^{\infty}\Bigg[\frac{2}{j\left[k+b\right]}J_k\left(c\frac{M}{2}\pi\right)\times\Bigg\{\cos\left([k+b]\frac{\pi}{2}\right)\sin\left([\mathrm{k\text{-}c}]\frac{\pi}{2}\right)\Big(\mathrm{e}^{j\frac{1}{2}([\mathrm{k\text{-}b}]\delta-5[k+b]\pi)} \\
&\quad +\mathrm{e}^{-j[k+b]\delta}-\mathrm{e}^{-j\frac{1}{2}[k+b][\delta+\pi]}-\mathrm{e}^{j(k\delta-[k+b]\pi)}\Big)-j2\cos\left([k+b]\frac{\pi}{2}\right)\sin\left([k+b]\frac{\delta-\pi}{4}\right)\sin\left([k+c]\frac{\pi}{2}\right) \\
&\quad \times\mathrm{e}^{-j\frac{1}{4}([-3k+b]\delta+3[k+b]\pi)}\Bigg\}\Bigg|_{k\neq-b}+\left(-\delta+\pi\right)J_k\left(c\frac{M}{2}\pi\right)\left\{\sin\left([\mathrm{k\text{-}c}]\frac{\pi}{2}\right)\left(1+\mathrm{e}^{jk\delta}\right)\right. \\
&\quad \left.+\sin\left([k+c]\frac{\pi}{2}\right)\mathrm{e}^{jk\delta}\right\}\Bigg|_{k=-b}\Bigg]+\frac{2V_{\mathrm{dc}}}{c\pi^2}\sum_{k=-\infty}^{\infty}\sum_{h=-\infty}^{\infty}\Bigg[\frac{4}{j\left[h+k+b\right]}J_k\left(c\frac{M}{2}\pi\right)\cos\left([h+k+b]\frac{\pi}{2}\right) \\
&\quad \times\Bigg\{jJ_h\left(c\frac{M}{2}\pi\right)\sin\left([h+k+b]\frac{\delta}{2}\right)\sin\left([h+\mathrm{k\text{-}c}]\frac{\pi}{2}\right)\mathrm{e}^{j\frac{1}{2}[h-\mathrm{k\text{-}b}]\delta}+jJ_h\left(c\frac{M}{2}\pi\right)\sin\left([h+k+b]\frac{\delta}{2}\right) \\
&\quad \times\sin\left([h-k+c]\frac{\pi}{2}\right)\mathrm{e}^{j\frac{1}{2}[h-\mathrm{k\text{-}b}]\delta}+J_h\left(cM\pi\right)\sin\left([h+k+b]\frac{\delta-\pi}{2}\right)\sin\left([h-k+c]\frac{\pi}{2}\right) \\
&\quad \times\mathrm{e}^{j\frac{1}{4}([h-3k+3b]\delta-[2+h+k+b]\pi)}\Bigg\}\Bigg|_{k+h\neq-b}+\mathrm{e}^{j\delta h}J_k\left(c\frac{M}{2}\pi\right)\left\{\left(-\delta+\pi\right)J_h\left(cM\pi\right)\sin\left([h-k+c]\frac{\pi}{2}\right)\right. \\
&\quad \left.+4\delta J_h\left(c\frac{M}{2}\pi\right)\cos\left([\mathrm{k\text{-}c}]\frac{\pi}{2}\right)\sin\left(h\frac{\pi}{2}\right)\right\}\Bigg|_{k+h=-b}\Bigg]
\end{aligned}
\tag{A.8}
$$

baseband harmonic components. The third case defines the carrier harmonic components. The final case represents the sideband harmonic components.

When $\boldsymbol{c} = \boldsymbol{b} = \mathbf{0}$ in case 1, (19) can be expressed as:

$$\begin{aligned} A_{00} + jB_{00} &= \frac{V_{dc}}{\pi^2} \sum_i \int_{y_s(i)}^{y_e(i)} \int_{x_r \mathrm{A}(i)}^{x_{fA}(i)} \mathrm{d}x\, \mathrm{d}y \\ &\quad - \frac{V_{dc}}{\pi^2} \sum_i \int_{y_s(i)}^{y_e(i)} \int_{x_r N(i)}^{x_{fN}(i)} \mathrm{d}x\, \mathrm{d}y \\ &= 0 \end{aligned} \tag{A.1}$$

where $\boldsymbol{x_{fA}(i)}$ and $\boldsymbol{x_{rA}(i)}$ are inner double Fourier integral limits for $\boldsymbol{V_{aN}}$, $\boldsymbol{x_{fN}(i)}$ and $\boldsymbol{x_{rN}(i)}$ is inner double Fourier integral limits for $\boldsymbol{V_{sN}}$.

When $\boldsymbol{c} = \mathbf{0}, \boldsymbol{b} \neq \mathbf{0}$ in case 2, the coefficients are only determined using $\boldsymbol{b}$ in this case because $\boldsymbol{c}$ is zero. For this case, (19) simplifies to

$$\begin{aligned} &A_{0b} + jB_{0b} \\ &\quad = \frac{V_{dc}}{\pi^2} \sum_i \int_{y_s(i)}^{y_e(i)} \int_{x_r \mathrm{A}(i)}^{x_{fA}(i)} e^{jby} \mathrm{d}x\, \mathrm{d}y \\ &\qquad - \frac{V_{dc}}{\pi^2} \sum_i \int_{y_s(i)}^{y_e(i)} \int_{x_r N(i)}^{x_{fN}(i)} e^{jby} \mathrm{d}x\, \mathrm{d}y = 2MV_{dc} \end{aligned} \tag{A.2}$$

For $\boldsymbol{c} > \mathbf{0}, \boldsymbol{b} = \mathbf{0}$ in case 3, the carrier harmonics included in the pole voltage are symmetrical to each other, and when the difference between the pole voltages is obtained, they cancel out.

When $\boldsymbol{c} > \mathbf{0}, \boldsymbol{b} \neq \mathbf{0}$ in case 4, (19) can be expressed as

$$\begin{aligned} &A_{cb} + jB_{cb} \\ &= \frac{V_{dc}}{\pi^2} \sum_i \int_{y_s(i)}^{y_e(i)} \int_{x_r \mathrm{A}(i)}^{x_{fA}(i)} e^{j(cx+by)} \mathrm{d}x \mathrm{d}y \\ &= \frac{V_{dc}}{\pi^2} \sum_i \int_{y_s(i)}^{y_e(i)} \int_{x_r N(i)}^{x_{fN}(i)} e^{j(cx+by)} \mathrm{d}x\, \mathrm{d}y \\ &= -\frac{2V_{dc}}{c\pi^2} \sum_i \int_{y_s(i)}^{y_e(i)} e^{jby} \left[2 \sin\left(cM\pi \cos y\right)\right. \\ &\quad + \sin\left(cM\pi \cos\left(y + \delta\right)\right) + \sin\left(c\pi + cM\pi \cos y\right) \\ &\quad - \sin\left(c\pi - cM\pi \cos y\right) - \sin\left(c\pi - cM\pi \cos\left(y + \delta\right)\right) \\ &\quad + \sin\left(cM\pi \cos y - cM\pi \cos\left(y + \delta\right)\right) \\ &\quad \left. + \sin\left(c\pi + cM\pi \cos y - cM\pi \cos\left(y + \delta\right)\right)\right] \mathrm{d}y \end{aligned} \tag{A.3}$$

To calculate the outer integral over $\boldsymbol{y}$ of (A.3), Euler's formula and Jacobi -Anger expansion needs to be used. And then (A.3) is finally equal to (A.4), as shown at the bottom of page 15. Applying the calculated coefficients for each harmonic component to (18), the complete harmonic solution can be expressed by (A.5), as shown at the bottom of page 15, for $\boldsymbol{a}$ phase voltage of proposed DPWM method. Moreover, the remaining complete harmonic solution for other phase voltages can be derived in a similar manner and the results are shown in (A.6), as shown at the bottom of page 15, (A.7) and (A.8), as shown at the bottom of the previous page.

REFERENCES

[1] "Sonar," in *Encyclopaedia Britannica*. Jan. 2019.
[2] J. E. Thorner, "Approaches to sonar beamforming," in *Proc. IEEE Southern Tier Tech. Conf.*, Binghamton, NY, USA, Apr. 1990, pp. 69–78.
[3] M. R. Arshad, "Recent advancement in sensor technology for underwater applications," *Indian J. Marine Sci.*, vol. 38, no. 3, pp. 267–273, 2009.
[4] D.-H. Jang and D.-Y. Yoon, "Space-vector PWM technique for two-phase inverter-fed two-phase induction motors," *IEEE Trans. Ind. Appl.*, vol. 39, no. 2, pp. 542–549, Mar. 2003, doi: 10.1109/TIA.2003.809448.
[5] D.-H. Jang, "Voltage, frequency, and phase-difference angle control of PWM inverters-fed two-phase induction motors," *IEEE Trans. Power Electron.*, vol. 9, no. 4, pp. 377–383, Jul. 1994, doi: 10.1109/63.318895.
[6] M. B. R. Correa, C. B. Jacobina, A. M. N. Lima, and E. R. C. Da Silva, "Field oriented control of a single-phase induction motor drive," in *Proc. Rec. 29th Annu. IEEE Power Electron. Spec. Conf. (PESC)*, Fukuoka, Japan, vol. 2, May 1998, pp. 990–999, doi: 10.1109/PESC.1998.703124.
[7] M. A. Jabbar, A. M. Khambadkone, and Z. Yanfeng, "Space-vector modulation in a two-phase induction motor drive for constant-power operation," *IEEE Trans. Ind. Electron.*, vol. 51, no. 5, pp. 1081–1088, Oct. 2004.
[8] S. S. Wekhande, B. N. Chaudhari, S. V. Dhopte, and R. K. Sharma, "A low cost inverter drive for 2-phase induction motor," in *Proc. IEEE Int. Conf. Power Electron. Drive Syst. (PEDS)*, Hong Kong, Jul. 1999, pp. 428–431.
[9] M. B. de Rossiter Correa, C. B. Jacobina, A. M. N. Lima, and E. R. C. da Silva, "A three-leg voltage source inverter for two-phase AC motor drive systems," *IEEE Trans. Power Electron.*, vol. 17, no. 4, pp. 517–523, Jul. 2002.
[10] D. G. Holmes and A. Kotsopoulos, "Variable speed control of single and two phase induction motors using a three phase voltage source inverter," in *Proc. 28th Conf. Rec. IEEE Ind. Appl. Conf. IAS Annu. Meeting*, Toronto, ON, Canada, vol. 1, 1993, pp. 613–620.
[11] C. M. Young, C. C. Liu, and C. H. Liu, "New inverter-driven design and control method for two-phase induction motor drives," *Proc. IEE-Elect. Power Appl.*, vol. 143, no. 6, pp. 458–466, 1996.
[12] V. Kinnares and C. Charumit, "Modulating functions of space vector PWM for three-leg VSI-fed unbalanced two-phase induction motors," *IEEE Trans. Power Electron.*, vol. 24, no. 4, pp. 1135–1139, Apr. 2009.
[13] C. Charumit and V. Kinnares, "Analogue space vector modulator for two-phase loads using a three-leg voltage source inverter," in *Proc. IEEE Int. Conf. Robot. Biomimetics*, Bangkok, Thailand, Feb. 2009, pp. 1607–1612.
[14] J.-H. Kim and S.-K. Sul, "A carrier-based PWM method for three-phase four-leg voltage source converters," *IEEE Trans. Power Electron.*, vol. 19, no. 1, pp. 66–75, Jan. 2004.
[15] A. M. Hava, R. J. Kerkman, and T. A. Lipo, "A high-performance generalized discontinuous PWM algorithm," *IEEE Trans. Ind. Appl.*, vol. 34, no. 5, pp. 1059–1071, Sep. 1998.
[16] V. Blasko, "Analysis of a hybrid PWM based on modified space-vector and triangle-comparison methods," *IEEE Trans. Ind. Appl.*, vol. 33, no. 3, pp. 756–764, Jun. 1997.
[17] K. Zhou and D. Wang, "Relationship between space-vector modulation and three-phase carrier-based PWM: A comprehensive analysis [three-phase inverters]," *IEEE Trans. Ind. Electron.*, vol. 49, no. 1, pp. 186–196, 2002.
[18] O. Ojo, "The generalized discontinuous PWM scheme for three-phase voltage source inverters," *IEEE Trans. Ind. Electron.*, vol. 51, no. 6, pp. 1280–1289, Dec. 2004.
[19] C. Charumit and V. Kinnares, "Discontinuous SVPWM techniques of three-leg VSI-fed balanced two-phase loads for reduced switching losses and current ripple," *IEEE Trans. Power Electron.*, vol. 30, no. 4, pp. 2191–2204, Apr. 2015.
[20] D. Christen and J. Biela, "Analytical switching loss modeling based on datasheet parameters for MOSFETs in a half-bridge," *IEEE Trans. Power Electron.*, vol. 34, no. 4, pp. 3700–3710, Apr. 2019.
[21] J. W. Kolar, H. Ertl, and F. C. Zach, "How to include the dependency of the $R_{DS(on)}$ of power MOSFETs on the instantaneous value of the drain current into the calculation of the conduction losses of high-frequency three-phase PWM inverters," *IEEE Trans. Ind. Electron.*, vol. 45, no. 3, pp. 369–375, Jun. 1998.
[22] T. Bruckner and D. G. Holmes, "Optimal pulse-width modulation for three-level inverters," *IEEE Trans. Power Electron.*, vol. 20, no. 1, pp. 82–89, Jan. 2005.
[23] S. Fukuda, K. Suzuki, and Y. Iwaji, "Harmonic evaluation of an NPC PWM inverter employing the harmonic distortion determining factor," in *Proc. 13th Conf. Rec. IEEE Ind. Appl. Conf. Annu. Meeting (IAS)*, Orlando, FL, USA, Oct. 1995, pp. 2417–2421.

[24] S. Bowes and B. M. Bird, ''Novel approach to the analysis and synthesis of modulation processes in power convertors,'' in *Proc. IEE*, London, U.K., May 1975, vol. 122, no. 5, pp. 507–513.
[25] F. P. Incropera and D. P. De Witt, *Fundamentals of Heat and Mass Transfer*. New York, NY, USA: Wiley, 1996.

JAEHYUK CHOI (Student Member, IEEE) was born in Daejeon, South Korea, in 1986. He received the M.Sc. degree in electrical engineering from Konkuk University in 2015, with a master's thesis focused on the linear motor propulsion system for railway applications, where he is currently pursuing the Ph.D. degree. His research interest includes the design of high-frequency converters such as SONAR systems.

DONG-HUN LEE received the B.Sc. and M.Sc. degrees from Kyungpook National University, Daegu, South Korea, in 1994 and 1996, respectively, and the Ph.D. degree from Pusan National University, Pusan, South Korea, in 2017. Since 1996, he has been a Senior Researcher with Agency for Defense Development.

HYUNGSOO MOK (Member, IEEE) received the B.Sc., M.Sc., and Ph.D. degrees from Seoul National University, Seoul, South Korea, in 1986, 1988, and 1992, respectively. He was with the Department of Control and Instrumentation Engineering, Seoul National Polytechnic University, as an Associate Professor, from 1993 to 1997. Since 1997, he has been with the Department of Electrical Engineering, Konkuk University, as a Full Professor. His current research interests include power electronics, machine control, and simulation techniques using PSpice and MATLAB.